International Atomic Energy Agency

INDC(CCP)-238
Distr.: L

INDC INTERNATIONAL NUCLEAR DATA COMMITTEE

# PROMPT NEUTRON ENERGY SPECTRUM FOR THE SPONTANEOUS FISSION OF CF-252

M.V. Blinov, G.S. Boykov and V.A. Vitenko

V.G. Khlopin Radium Institute
Leningrad, 197022, USSR



1984

IAEA NUCLEAR DATA SECTION, WAGRAMERSTRASSE 5, A-1400 VIENNA

Reproduced by the International Atomic Energy Agency
Vienna, Austria
June 1985

85-02906

Translated from Russian

# PROMPT NEUTRON ENERGY SPECTRUM FOR THE SPONTANEOUS FISSION OF CF-252*)

M.V. Blinov, G. S. Boykov and V. A. Vitenko
V.G. Khlopin Radium Institute
Leningrad, USSR

(1984)

## Abstract

The prompt neutron spectrum for the spontaneous fission of Cf-252 has been measured in 0.01-10 MeV region by the time-of-flight technique using a fast ionization chamber with U-235 layers as the neutron detector. Numerical data for the spectrum are presented, with an error file.

*) The work was carried out under IAEA Research Agreement 2791/CF

## 1. INTRODUCTION

The study of the neutron spectrum for Cf-252 spontaneous fission in a wide energy region (1 keV-20 MeV) is a actual problem of topical relevance. This spectrum has been recommended by the IAEA as an international neutron spectrum standard. For purposes of in-core reactor dosimetry, the evaluation of Grundl and Eisenhauer /1/ based on a number of experimental studies up to 1975 was used in IRDF-82 /2/ as the recommended shape of the spectrum. In the last few years new experimental studies /3, 4, 5/ have appeared, where the measurement accuracy was higher and the energy region of measurement wider. However, the short descripton of the measurement techniques and the results makes it difficult to analyse the errors in detail with a view to obtaining new evaluated data.

Our studies /6, 7/ carried out at the V.G. Khlopin Radium Institute also contained a short description of the measurements and the results obtained with a neutron detector based on the U-235(n,f) reaction, the cross-section of which is used as the standard. As the "zero time" detector we used a miniature current ionization fission chamber giving a high time resolution.

The purpose of the present work was to describe in detail the procedure of preparation, checking and calibration of the neutron source, fragment and neutron detectors and of the spectrometer as a whole. We have tried to give a fuller description of the measurement procedure, treatment and introduction of corrections, with an analysis of the possible errors.

The measurement results obtained were compared with the results of the experimental study /8/, which was based on the neutron detector with using the standard Li-6(n,$\alpha$) cross-section, and also with the calculations contained in Refs /9-11/.

## 2. METHOD

For the purpose of measurements we chose the time-of-flight technique since it can give a high energy resolution over the whole of the neutron energy region under study. Moreover, it has the advantage of being based on the unique correspondence between the time-of-flight and neutron energy. Another common method which is based on recording the amplitude distribution of pulses

from recoil nuclei does not use the direct correspondence of values but requires an accurate knowledge of the response function, which is complicated to measure.

For the time-of-flight technique to be applicable it is necessary to determine the instant of neutron emission with a sufficiently high accuracy. The bulk of the fission neutrons are emitted in a time interval smaller than $10^{-14}$s after the fission event. A very small number of neutrons, emitted possibly in somewhat longer times, may have a very small influence on the measurement results.

The instant of emission of spontaneous fission neutrons is detected usually on the basis of the associated particles - fragments or gamma quanta. The use of gamma quanta as the associated particle reduces the fission event registration efficiency; moreover, it is necessary to have experimental proof of the absence of a correlation between gamma quanta and neutrons. We also note that, in this case, we bare the problem of designing a high-efficiency gamma quantum detector which would cause a low destortion in the fission neutron field by scattering. The best method is to detect fission fragments. The principal requirement in this case is that there should be no selection of fragments with respect to energy or angle of emission since a correlation exists between these values and neutron energy. Evidently the best method is to register fragments within an angle $2\pi$ with an efficiency close to 100 %.

At present, it can be assumed that there are no grounds for doubting the applicability in principle of the time-of-flight technique to the given problem although the results obtained by this technique differ significantly from each other. We believe that the reason for the latter lies in the specific conditions of the technique - operation of the experimental facilities, influence of measurement conditions and so on.

The bulk of the studies in the 0.5-15 MeV region were carried out with organic scintillators as neutron detectors. These detectors not being suitable for the region of lower energies, we chose a non-threshold detector based on the exothermal reaction U-235(n,f) whose cross-section is used as the neutron standard. The accuracy of this standard has been increasing every year, and at present it is not lower than 2-4 % for the 100 keV-15 MeV region /12/.

## 3. SOURCE OF SPONTANEOUS FISSION NEUTRONS - THE CF-252 LAYER

For precision measurements of fission neutron spectra it is very important to have a Cf-252 layer with a high degree of purity and quality of preparation. In the initial sample which was used for preparing the sources the total contribution of spontaneous fissions from curium and californium isotopes relative to Cf-252 was $\sim 5 \times 10^{-4}$. In this case, the major share belonged to the fission of Cf-250. Since the contribution by the spontaneous fission of nuclides other than Cf-252 is small and the fission neutron spectra are similar in shape, destortion of the Cf-252 spectra due to this reason is negligibly small. We note that the californium source also emits neutrons as a result of the $(\alpha,n)$ reaction; however, their yield is small and they are not recorded by the coincidence method but only increase the neutron background.

The sources were obtained by depositing the Cf-252 preparation on platinum backing by vacuum sputtering. The backing with a thickness of 0.1 mm was polished in advance to a high surface purity (average roughness of the surface - 0.15 μm), which was determined with an interferometer. The evaporator was a tantalum strip with a hemispherical depression 4 mm in diameter, to which an aliquot of the initial californium prepration was applied. In order to eliminate the volatile impurities, we pre-heated the evaporator at 1000°C. The californium preparation was evaporated at a temperature of 1600-1700°C and a pressure of $10^{-4}$ mm Hg. On the backings the Cf-252 was sublimated in the form of the oxides CfO and $Cf_2O_3$. The homogeneity of the obtained layers 4 mm in diameter, measured by alpha scanning, was $\sim 10$ %. In this manner sources of different weights from 0.01 to 1 μg were prepared.

The absolute weights of the sources were determined by recording the number of fissions within a small solid angle. Moreover, the weights were also determined by measuring the absolute neutron yields and using the value of $\bar{\nu}$ for Cf-252, which is the international standard (accuracy higher than 0.5 %). The neutron

yield was determined with the help of a manganese bath, used in the intercomparisons (0.5 % accuracy of determination) /13/. Then the quality of the deposited Cf-252 layer was checked by measuring the fragment yields at different angles to the backing plane in a vacuum chamber, using semiconductor detectors. The angular resolution was 1°.

Figure 1 shows the typical energy distributions of fragments for emission angles of 4 and 41° to the backing plane. The spectrum quality is quite satisfactory - the ratio of the light fragment peak to the valley for a 45° angle was ~2.7. In the case of angles of 45° and smaller we observe a regular shift of the spectra towards the low energy region and also an effective back-scattering of fragments from the backing (in the energy region below 50 MeV). This effect leads to an increase in the integral count of the fragments. Figure 2 gives the results of processing of the angular differential spectra in the form of the integral count as a function of the angle of emission of fragments for two thresholds ($B_1$ = 15 MeV and $B_2$ = = 45 MeV). The result obtained at a registration threshold of $B_2$ indicates that for fragment emission angles greater than 2° there is no absorption of fragments in the layer. This demonstrates that the quality of the layer in the working sources was perfectly satisfactory.

Although the quality of the californium layers was high immediately after preparation, it was necessary to ensure that their quality would not change appreciably during a prolonged experiment. In order to determine the influence of the time factor on the layer quality, we made control measurements for californium layers which had been kept for different periods after deposition on the backing. It was found that the quality deteriorated with time and that the coefficient of deterioration increased substantially for sources with a high density of the californium layer. For example, in the case of a layer with a weight of 1 $\mu$g (4 mm in diameter) about 10 % of fragments at an angle of 4° were not recorded two years after preparation. In our experiment the "ageing" factor did not noticeably affect the layer quality.

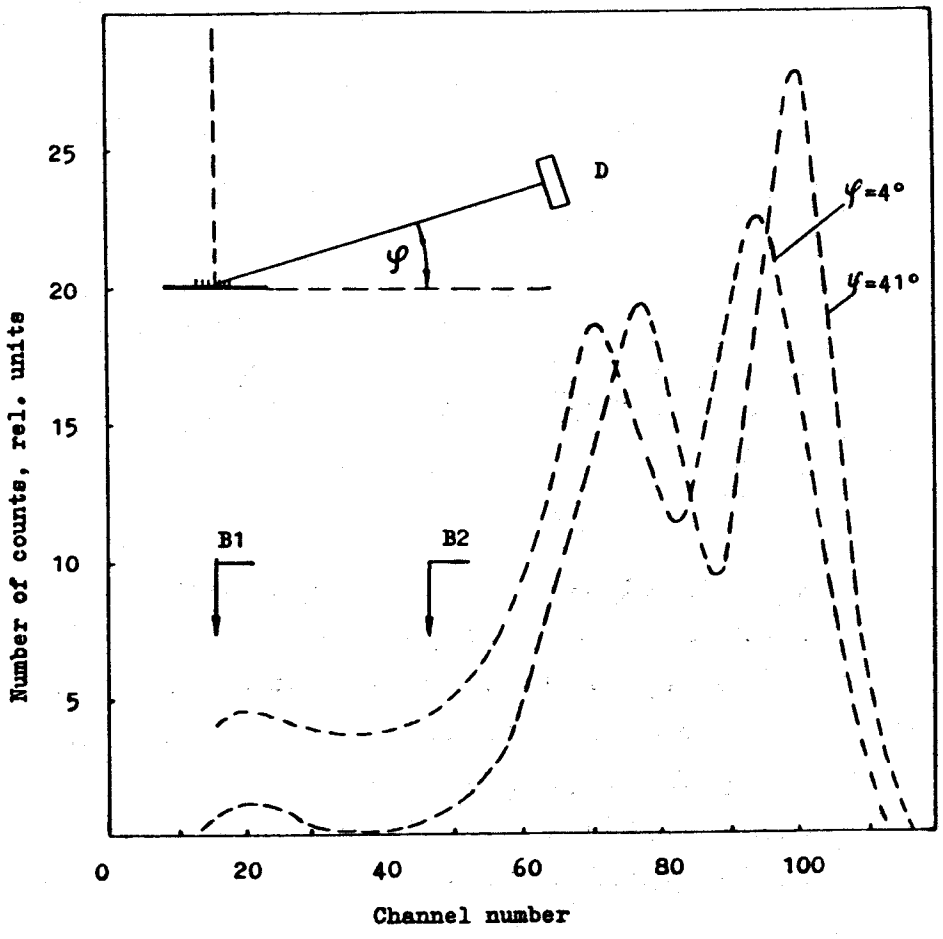


Figure 1 The fragment amplitude spectra for two angles of emission: $\varphi_1 = 4°$ and $\varphi_2 = 41°$. The arrows indicate $B_1 = 15$ MeV and $B_2 = 45$ MeV, the thresholds of the integral discriminators.

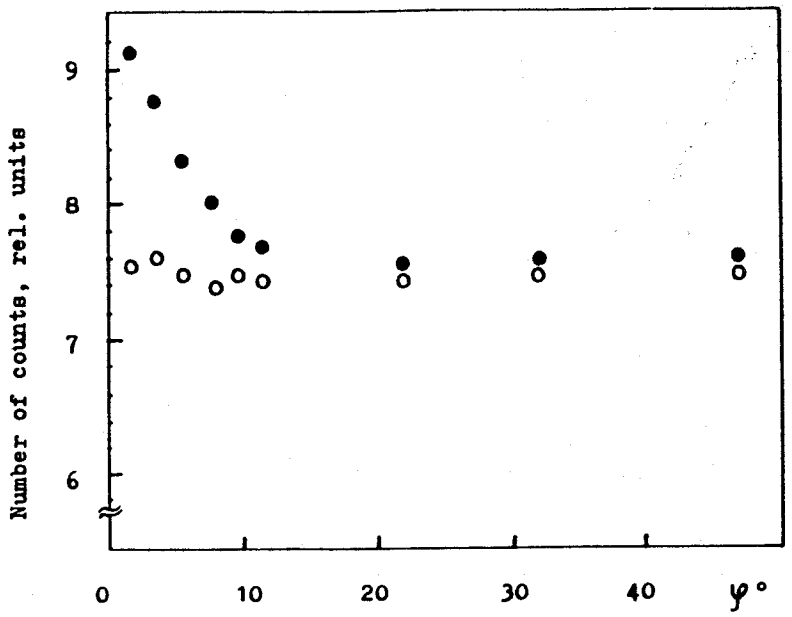


Figure 2 The integral dependences of fragment counts on emission angles for two registration thresholds (● - $B_1$ and o - $B_2$).

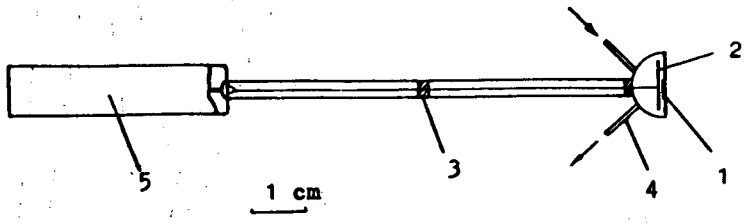


Figure 3 Diagram of the current ionization chamber together with the preamplifier:
(1) - Cf-252 layer on platinum backing;
(2) - current-collecting platinum electrode;
(3) - fluoroplastic insulator;
(4) - capillary inlets for pumping methane;
(5) - preamplifier.

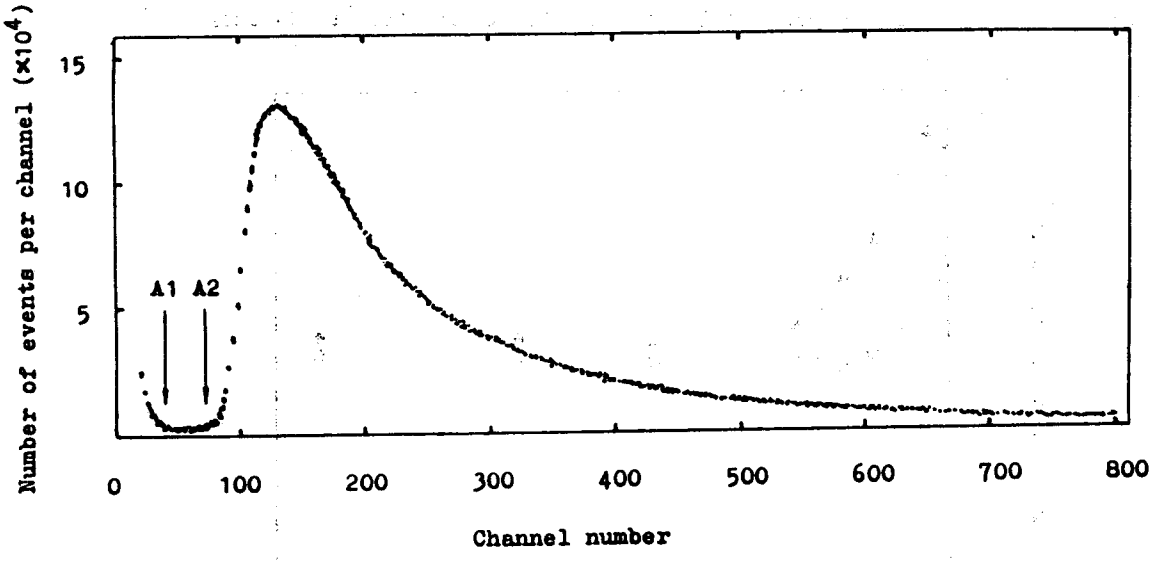


Figure 4 The fragment amplitude spectrum of the californium fission chamber. $A_1$ and $A_2$ are the thresholds of the integral discriminator.

## 4. SPONTANEOUS FISSION FRAGMENT DETECTOR

Fission neutron spectra can be measured with a U-235 layer as a neutron detector only when the neutron source intensity is very high since in this case the neutron spectrometer has a very low efficiency (for example, for a 50 cm path length $\varepsilon \simeq 10^{-7}$). We therefore used a Cf-252 source with an intensity of 4.51 x x $10^5$ fissions/s. At such a source intensity the most suitable fragment detector is the current ionization chamber. It is very fast-acting and gives a high time resolution. It can be small in size and weight. Such a chamber does not introduce much distortion into the neutron field of the source /14/. When constructing the chamber we tried to ensure a time resolution higher than 1 ns, a fragment recording efficiency close to 100 % and smaller chamber and preamplifier weights. A diagram of the chamber together with the preamplifier is shown in Fig. 3.

The chamber consists of a 16 mm hemisphere made of stainless steel (0.1 mm thick), to the end of which we soldered a platinum backing (0.1 mm thick) with a Cf-252 layer deposited on it. The collecting electrode (14 mm in diameter) was made of platinum (0.1 mm in thickness). The distance between the collecting electrode and the backing was 2 mm. The signal from the electrode (2) arrived via a cable with an air insulator at the preamplifier located at a distance of 10 cm from the Cf-252 layer. Methane was pumped at atmospheric pressure through capillary inlets. The total weight of the chamber together with the cable was 1.4 g. The capacitance of the current-collecting electrode together with the air cable was 3.5 pf. The time properties of the chamber depend to a considerable extent on the capacitance of the chamber and on the input characteristics of the preamplifier. Since the preamplifier should be very close to the chamber (in order to decrease cable capacitance), its weight should be minimal. We therefore designed a special preamplifier with an amplification factor of $\sim 100$ and a transmission band to $10^8$ Hz. The intrinsic noise of the amplifier together with the chamber (in recalculating to the input) was 34 x $10^{-6}$ V. The weight of the

preamplifier was 5.1 g. The pulse from the current chamber (together with the amplifiers) had a duration of 25 ns and the rise time 3.5 ns.

Figure 4 shows the amplitude spectrum of fragments from the chamber with a californium layer. It will be seen that the separation of fragment pulses from alpha particles and noise of the preamplifier is good. The recording of the pulse counting intensities at the two thresholds of the fast integral discriminator $A_1$ and $A_2$ ($A_2 = 2A_1$, see Fig. 4) showed that they differed from each other by not more than 0.5 %. This indicates that the possible proportion of undetected fragments in the chamber at a threshold of $A_1$ does not exceed 0.5 %.

A comparison was also made of the measured intensities of fissions in the same layer obtained under different conditions - in $2\pi$ geometry in the ionization chamber and at small solid angles (by the semiconductor detector) in the vacuum chamber. The measurement results with allowance for the "dead" time of the system agreed with an accuracy of 1 %.

In Refs /3, 4/ it was noted that there was a considerable variation in the number of detected fragment - neutron concidences as a function of the neutron emission angle with respect to the backing plane. In our case, the ratio of the number of registered neutrons (in coincidence with fragments) moving along the backing and those perpendicular to it is N (4°)/N (90°) = = 0.99 $\pm$ 0.01. This value was obtained with a backing 14 mm in diameter and 0.1 mm in thickness. In the measurements, the neutron detector was a stilbene crystal (50 x 50 mm) and the photomultiplier FEU-30 with $n/\gamma$ separation. The threshold was 0.47 MeV. The measurements were performed with a flight path length of 57 cm. For a more detailed study of the cause of the decrease in counts at 0° we performed control measurements with another backing with a larger diameter and thickness (diameter 24 mm, thickness 0.4 mm and layer intensity $5.5 \times 10^5$ fissions/s). As will be seen from Fig. 5, the fragment-neutron recording efficiency is practically independent of the neutron emission angle for 90-7,5°; at smaller angles, there is appre-

ciable scattering of neutrons in the backing. The calculated values of scattering showed good agreement with experimental data.

## 5. NEUTRON DETECTOR

Our neutron detector was a fast ionization chamber with U-235 layers. This type of detector has the following advantages: (1) It is a non-threshold detector with a smooth and relatively small variation in recording efficiency; (2) It is not sensitive to gamma quanta; (3) It has a well-known neutron recording efficiency (U-235 fission cross-section used as the standard).

One of its disadvantages is low efficiency. In order to make use of its positive characteristics, we had to: (1) Build a chamber of sufficiently light design with uranium layers (total weight of uranium $\sim 1$ g); (2) Obtain a time resolution of $\sim 1$ ns with such a chamber; (3) Obtain a high fragment recording efficiency with good separation from alpha particles.

Since in the present work we aimed at substantially decreasing the scattered neutron background and increasing the time resolution, we designed a chamber the diagram of which is shown in Fig. 6. As electrodes (100 mm in diameter) we used an aluminium foil with a thickness of 0.05 mm, on both sides of which were deposited layers of uranium containing 99.9 % of the U-235 isotope.

During the preparation of the layers by multiple deposition of the organic uranyl nitrate solution followed by annealing of each layer at 550°C, special attention was paid to achieving homogeneity in thickness, which depends in particular on the stability of the stoichiometric composition of the salt. The degree of homogeneity was determined from the alpha activity of the different parts of the layer, which was measured with a semiconductor detector. Figure 7 shows the homogeneity of the layer thickness as a function of target radius. Altogether

40 two-sided targets with an average layer thickness of 1.09 ± ± 0.05 mg/cm$^2$ were prepared. To improve current collection, we coated each layer with gold (thickness 0.05 mg/cm$^2$) by vacuum thermal sputtering.

Since at small flight path lengths the uncertainty in path length due to detector thickness makes an appreciable contribution to the energy resolution, it was necessary to make the gap between the electrodes as small as possible; however, a reduction in the spacing between electrodes results in a higher capacitance of the chamber and this in its turn proportionally increases the noise amplitude of the amplifier, and thereby impairs time resolution. In Figure 8 we have shown the dependence of the preamplifier noise amplitude as a function of chamber capacitance. In our case, with five plates and a 3-mm gap between the plates, the chamber capacitance ($C_k$) was 160 pf. The central and two outermost electrodes were current collectors, to which a high voltage of 400 V was applied. The latter was made of thin cadmium (0.2 mm in thickness) so that the background due to thermal neutrons was considerably reduced. The weight of the fully assembled chamber together with the preamplifier was 65 g. We used the same preamplifier as in the case of the californium chamber. The fission fragment pulse lasted 40 ns, the rise time lasted 6 ns. The working gas was methane, which was pumped continuously at atmospheric pressure through the working volume during the measurement.

Figure 9 shows the amplitude spectrum obtained in measurements with the working chamber in the fission neutron flux. The arrow indicates the recording threshold at which the spectrum measurements were performed. The threshold was set sufficiently high in order to reduce the background of alpha particles and noise. The fraction of fragments whose energy was lower than the threshold (in Fig.9 they are represented by the dashed curve) was determined by subtracting the contribution of alpha particles and preamplifier noises. The value of this fraction was 7.3 %. 9.3 % of the fragments from the working layers did not find their way inside the chamber because of absorption in

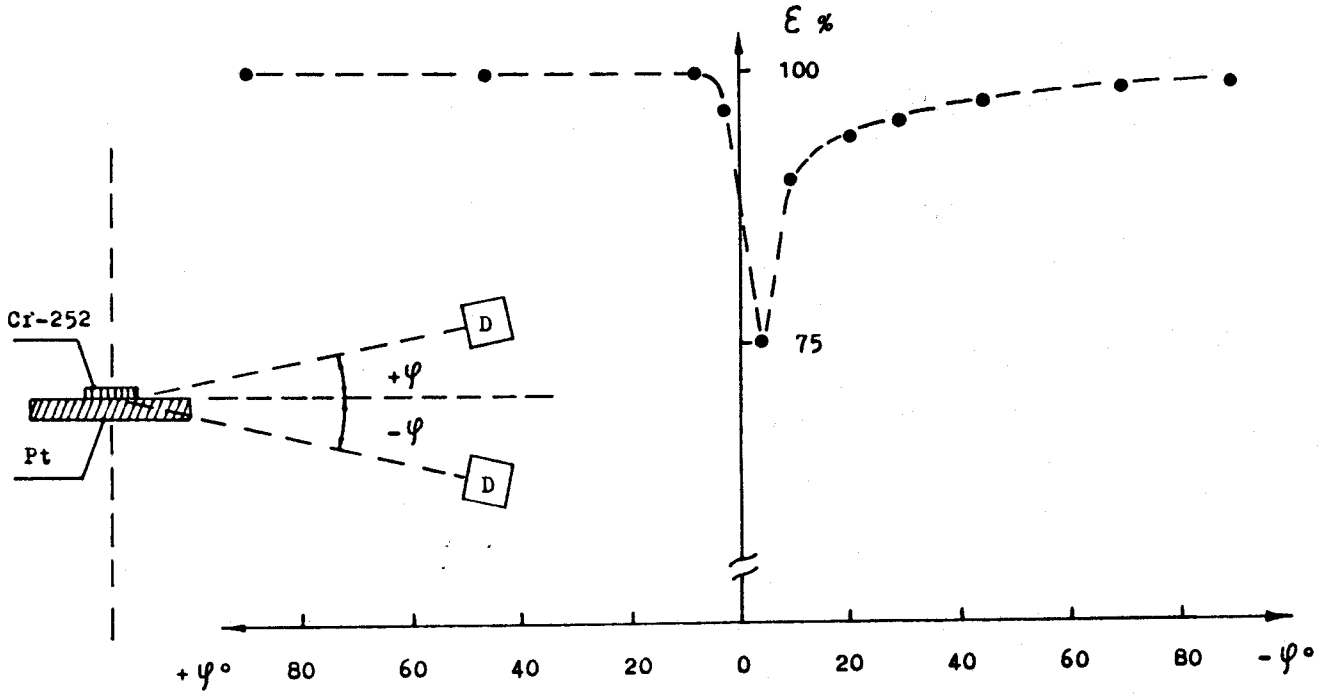


Figure 5 The efficiency of detecting fragment-neutron coincidences as a function of the neutron emission angle with respect to the backing plane. D is the neutron detector.

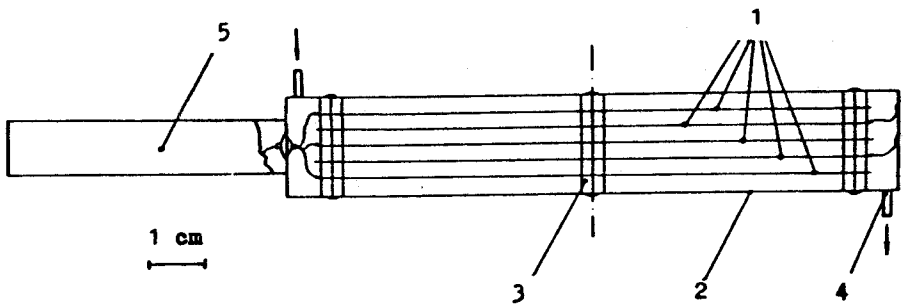


Figure 6 Diagram of the uranium chamber together with the preamplifier:
(1) - U-235 layer on aluminium backing;
(2) - cadmium shell;
(3) - fluoroplastic collars;
(4) - capillary inlets for pumping methane;
(5) - preamplifier.

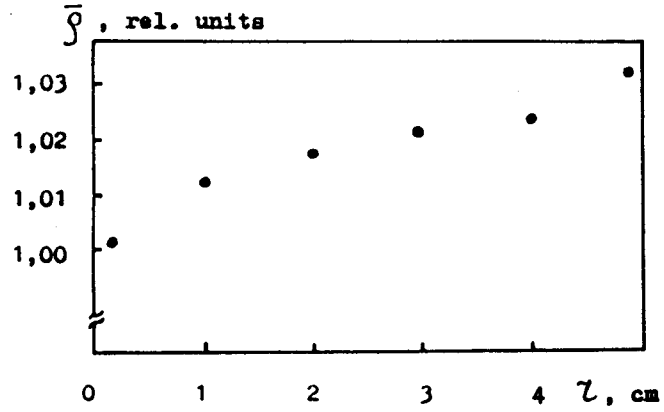


Figure 7 The average density of the uranium layer as a function of target radius. The density in the target centre is taken as one.

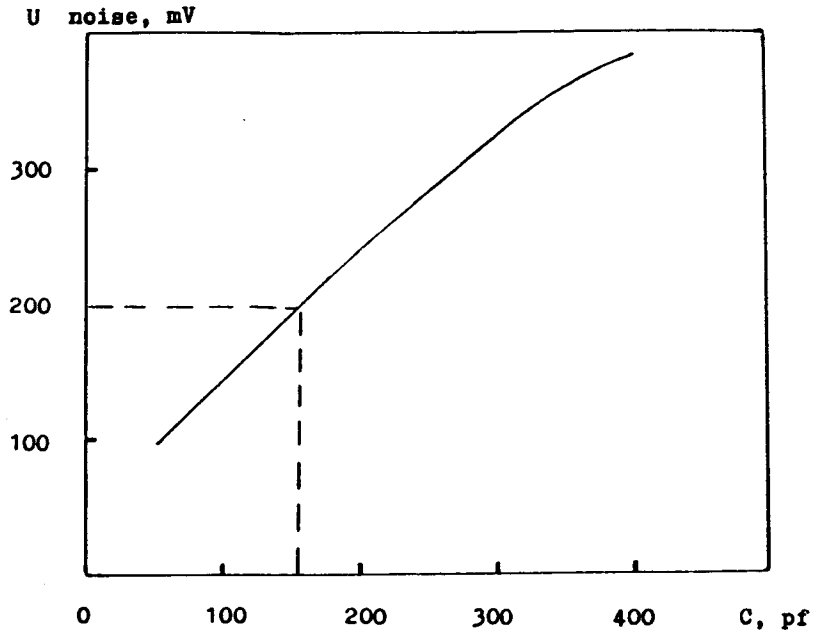


Figure 8 The amplitude of preamplifier noise as a function of fission chamber capacitance.

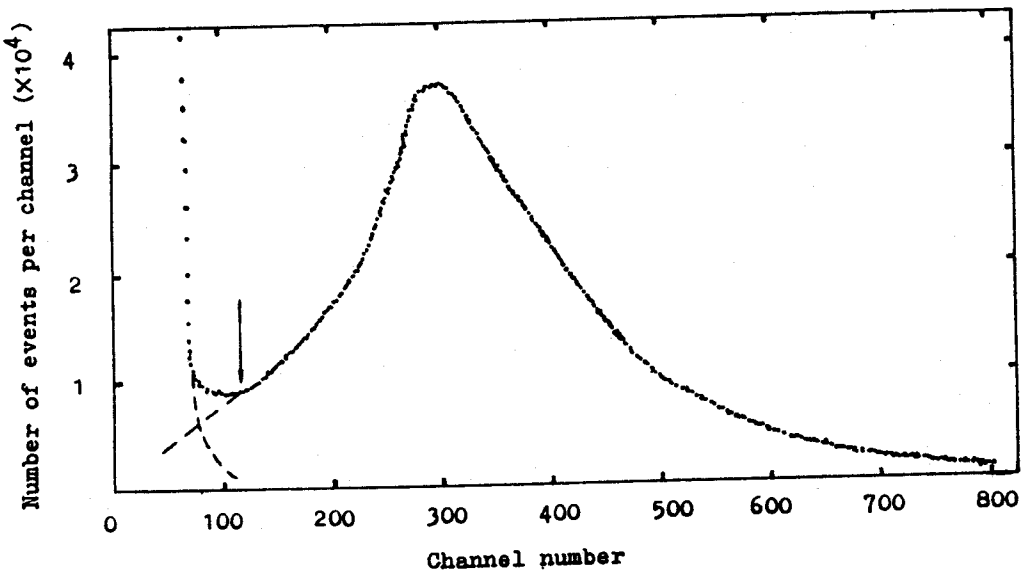


Figure 9 Fragment amplitude spectrum of the uranium chamber in the fission neutron flux. The arrow indicates the discriminator working threshold.

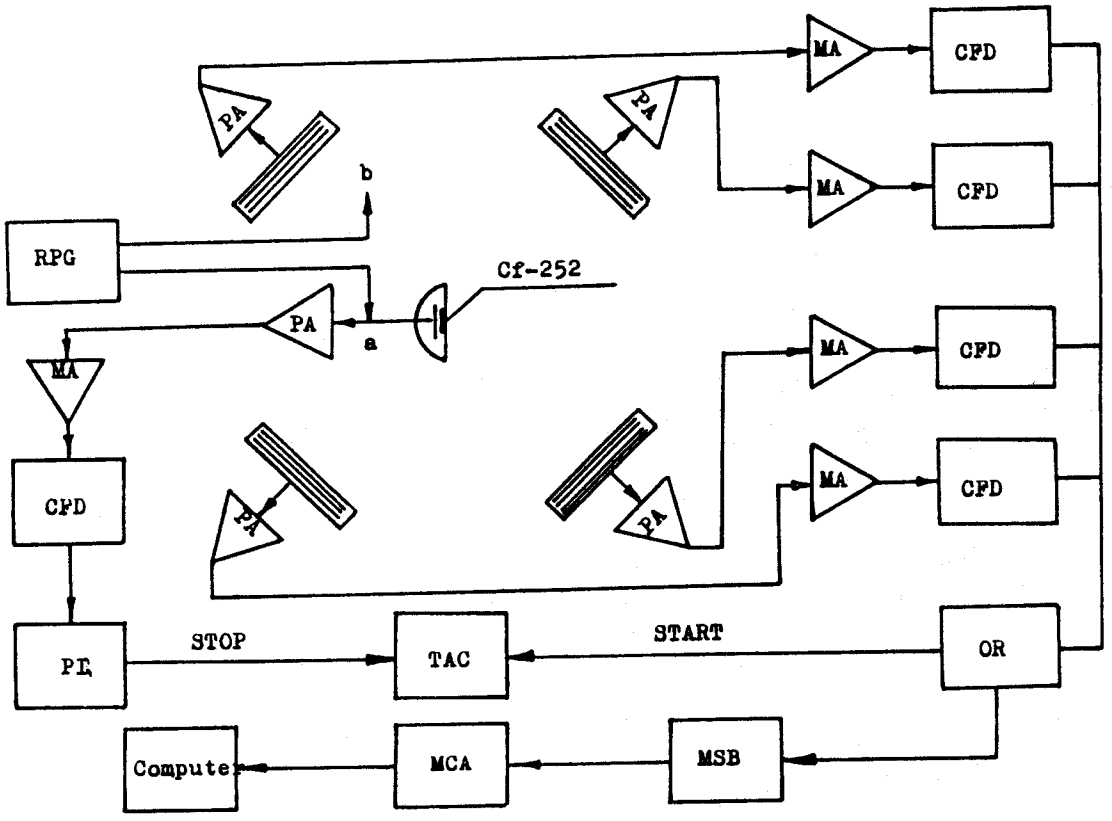


Figure 10 Block diagram of the spectrometer: PA - preamplifier; MA - main amplifier; CDF - constant fraction discriminator; MSB - memory separation block; RPG - reference peak generator; PR - pile-up-rejector; TAC - time-to-amplitude convertor; MCA - multichannel analyser.

uranium (without allowance for kinematic effects and anisotropy): this will be discussed in Section 7.4. Thus, the fragment recording effeciency was about 80 %. The intrinsic background of the chamber was $2 \times 10^{-3}$ pulses/s (under working conditions). This low background was due, first of all, to the high purity of the initial uranium preparation, the high percentage content of U-235, and fairly good separation of the fission fragment pulses from alpha particles and noises. The intrinsic background was determined mainly by the spontaneous fission of uranium nuclei in the chamber and by the pile-up of the pulses from the alpha decay of uranium. In the working measurements a considerable part of the random coincidence background was determined by the Cf-252 spontaneous fission delayed neutrons. The contribution of the $(\alpha,n)$ reaction was much lower.

## 6. ELECTRONIC SYSTEM OF THE SPECTROMETER

### 6.1. Spectrometer block diagram

At the first measurement stage, to increase the efficiency, of the neutron spectrometer, we used simultaneously four uranium chambers positioned at an angle of 45° relative to the plane of the californium layer backing (Fig. 10). Mixing of the linear signals from the chambers was not desirable since this increases noise and impairs the time resolution. At the second stage, we employed only one uranium chamber since this improved the time resolution. The fast signals from the chambers arrived at the main amplifiers via cables with a double screen. The double screening fully eliminated electrical induction due to various disturbances in the experiment room. The main amplifiers consisted of four cascades, connected in the "Rachet" circuit, with deep AC and DC negative feedback, which ensured high stability and linearity of the amplification factor ($\sim 350$) at a dynamic signal range of $\sim 100$ with a maximum amplitude of $\sim 6$ V. The upper limit of the amplification frequency was $5.0 \times 10^7$ Hz for

the amplifier of the uranium chamber and $10^8$ Hz for that of the californium chamber. Such a difference was necessary in order to obtain a better signal-to-noise ratio in both (neutron and fragment) channels. From the output of the main amplifiers the signals went to the circuits of the constant fraction discriminators (CFD) /15/, to which we introduced corrections for the matching of the time of actuation of the integral discriminator and the point of intersection of the given threshold. These changes, together with the good separation of fragments from alpha particles and noise in the amplitude distributions of the chambers (see Figs. 4 and 9), enabled us to avoid using the slow spectrometric channel. From the outputs of the CFD blocks (neutron) the signals were mixed by the "OR" circuit and went to the "START" input of the time-to-amplitude convertor (ORTEC-467). At the same time, the "OR" circuit generated signals to the memory separation block of the 4096-channel analyser (NORLAND-5400). This made it possible to record the spectra from each chamber separately to the corresponding quadrant of the analyser memory and to check thereby the operation of each of the four time channels.

## 6.2. Time interval rejector

At a Cf-252 source intensity of $5 \times 10^5$ fissions/s there is a distinct probability ($\sim$10 %) of more than one event (fission) occurring over the measured time interval ($\sim 2 \times 10^{-7}$ s). This will lead to a distortion of the spectrum, the value of the distortion being associated with the true shape of the spectrum and the intensity of the event. In Figure 11 we show the instrument spectrum obtained with a spectrometer where the neutron detector is a stilbene crystal and the FEU-30 and the "zero" detector is a current ionization chamber with a Cf-252 layer having an intensity of $5.5 \times 10^5$ fissions/s. At a recording threshold of $\geq$ 2 MeV there is no background before the spectrum (channel numbers less than 200), while the background after the spectrum has a substantial value. In a case

where the dead time of the fragment detector and electronics can be disregarded, from the formula in Refs /16, 17/ we can determine the true value of the distribution for any i-th channel:

$$F_i = e^{N_o t_i} \left[ N_i - N_o \tau_k \sum_{j=i+1}^{i_{max}} (N_j - N_{i\ max}) \right] \qquad (6.2.1)$$

where $N_o$ is the intensity of the Cf-252 source, $N_i$ the intensity of the spectrum in the i-th channel, $\tau_k$ the value of the channel, $N_{i\ max}$ the random background and $t_i$ the time of the i-th channel.

In Figure 11 the continuous curve (a) shows the dependence of the background associated with superposition of two fission events in the measured time interval. In neutron spectrum measurements where the intensity of the spectrum drops sharply with a decrease in energy, the recycle neutron background may exceed the effect. Therefore, we had earlier made and used a device /18/ which considerably reduced, and sometimes fully eliminated this background. The latest modification has been described in Ref /19/. The operating principle of this device is as follows. A short pulse (duration less than 10 ns) from the output of the CFD block successfully started two univibrators whose output pulses were mixed in the "OR" circuit, forming a blocking pulse which lengthened the delayed input signals for the transmission circuits, the delay time being somewhat longer than the duration of the blocking pulse. Thus, the input pulse rejection circuit transmitted only those input signals which were not preceded or followed by other pulses in a time interval smaller than the conversion time ($T_o$) of the time-to-amplitude convertor (TAC). If the interval between the pulses was smaller then time ($T_o$), both pulses were forbidden.

Since the "STOP" channel has a dead time ($\tau_d$ = 25 ns), i. e. the time during which there may occur two events but one pulse, the pile-up rejector will not exclude this pulse. As a result, some fraction of distortion associated with dead time ($\tau_d$) will be left in the neutron spectrum. The correction for dead time in the spectrum was calculated by the formula:

$$M(j+1) = N_o \tau_k \sum_{i}^{j} N_c \qquad i = \begin{cases} j - \dfrac{\tau_M}{\tau_k} & \text{for } j > \dfrac{\tau_M}{\tau_k} \\ 0 & \text{for } j \leqslant \dfrac{\tau_M}{\tau_k} \end{cases} \qquad (6.2.2)$$

where M(j+1) is the value of correction in the (j+1)-th channel, $\tau_k$ - the value of the channel, $N_o$ - the number of fissions in the layer, $\tau_d$ - the dead time (25 ns) and $N_c$ - the number of counts in the i-th channel.

In order to take accurate account of this effect, we made an experimental study of the value of the correction. The neutron spectrum measurements were performed with and without an rejector with source of $3.33 \times 10^5$ fissions/s and also without an rejector with a small source of $1.4 \times 10^3$ fissions/s.

In Figure 11 the value of this correction is shown by curve (6). Subtracting this correction from the experimental data obtained with the rejector, we find good agreement to within statistical errors with the data for the small source intensity where the value of the background due to the pile-up is decreased by a factor of more than 20.

In Ref /18/ we constructed a rejector system in the fragment channel (gas scintillation counter) without a dead time, introducing in addition the pulse amplitude analysis. This was possible because of the weak dependence of the signal amplitude on the energy and site of emission of the fragment (the dynamic range of amplitudes was less than 2). In the case of a plane current fission ionization chamber the dynamic amplitude range was more than $\sim 10$ (see Fig. 4). Therefore, for the purpose of amplitude rejection it is necessary to reduce the dynamic amplitude range to two.

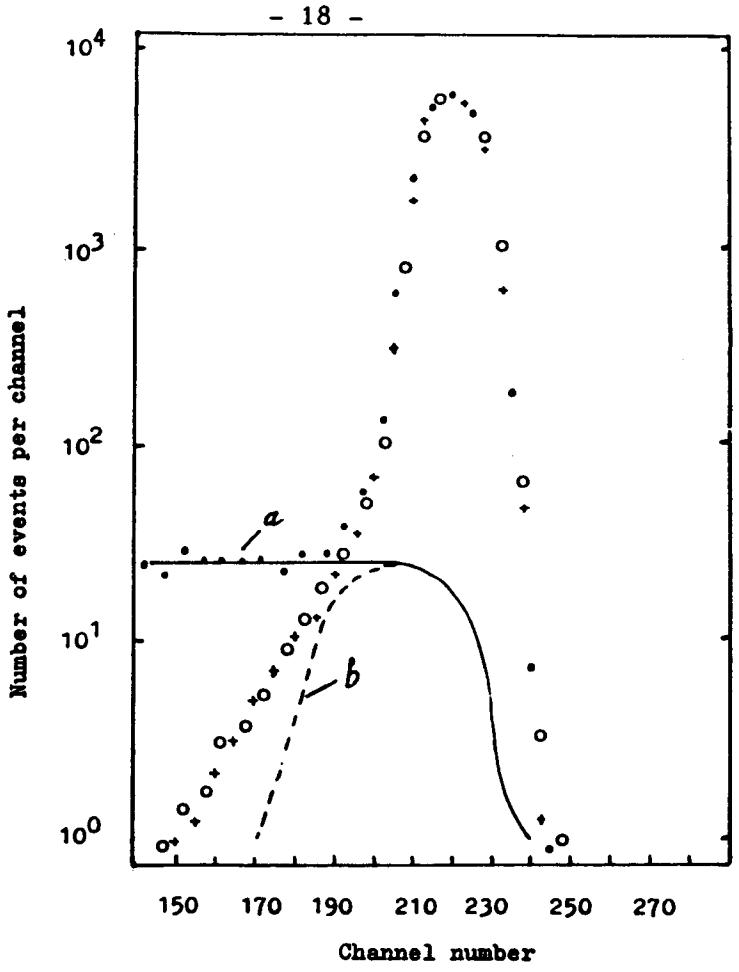


Figure 11 Time-of-flight spectra: ● - without pile-up rejector with a source intensity of $N_{01} = 3.33 \cdot 10^5$ fissions/s; o - with pile-up rejector and $N_{01}$; + - without pile-up rejector with $N_{02} = 1.45 \cdot 10^4$ fissions/s. Curve (a) is the background due to true-random coincidences without the pile-up rejector and curve (b) the background with the pile-up rejector.

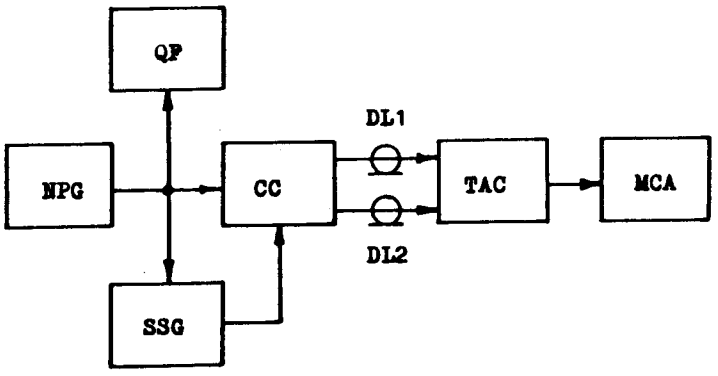


Figure 12 Block diagram of time interval calibration: NPG - nanosecond pulse generator; QF - quartz frequency meter; SSG - strobe signal generator; CC - coincidence circuit; DL1 and DL2 - delay lines; TAC - time-to-amplitude convertor; MCA - multichannel analyser.

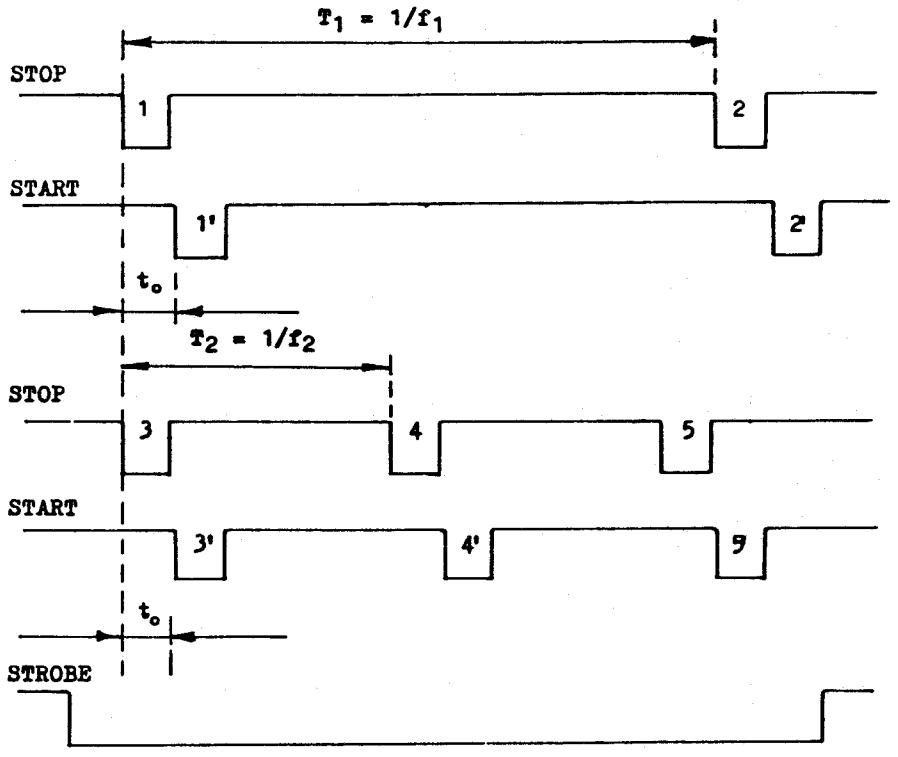


Figure 13 Time diagram (see Section 7.1) for the method of the time interval calibration.

## 7. CHARACTERISTICS OF THE SPECTROMETER

### 7.1. Spectrometer time scale

In order to measure the time-of-flight spectrum correctly, we need to have an accurate knowledge of the spectrometer time scale (channel time width). The common method of determining this scale involves the use of the standard delay lines. However, in some studies (for example, Ref /20/) the calibration by the delay line method did not coincide with those by other methods.

In the present work, we used two methods to increase the reliability - the method of standard delay lines and that of calibrated time intervals. The latter method consists of the following (the block diagram of the measurements is shown in Fig. 12). The nanosecond generator of pulses (NPG) with a rise time of $\sim 3$ ns and a variable repetition frequency starts the strobe signal generator (SSG), which was phased in such a way that the beginning of the strobe signal always was between the generator pulses (see Fig. 13). The duration of the strobe signal should be somewhat longer than the TAC conversion time interval ($T_o$) and the frequency $\sim 10^2$ Hz. Then, through the coincidence circuit (CC) there will pass pulses whose periods will be shorter than the duration of the strobe pulse. The "START" and "STOP" of the TAC will be fed pulses through delay lines DL1 and DL2 whose values are so chosen that the following condition is satisfied:

$$t_{DL1} - t_{DL2} = t_o > t_p$$

where $t_p$ is the duration of the pulse from the NPG output equal to 10 ns.

Choosing the repetition frequency of the NPG so that:

$$T_1 = \frac{1}{f_1} \lesssim T_o \quad - \quad \text{VARIANT I}$$

$$T_2 = \frac{1}{f_2} \ll T_o \quad - \quad \text{VARIANT II}$$

Then, on the multichannel analyser scale there will be two peaks with channel numbers $N_1$ and $N_2$, respectively. Since $N_1 \sim T_1 - t_o$ and $N_2 \sim T_2 - t_o$, therefore $T_1 - T_2 \sim N_1 - N_2$ and $\frac{1}{f_1} - \frac{1}{f_2} = T$. The frequency of the generator (NPG) is measured with a quartz frequency meter (QF). Knowing the difference of frequencies, we can determine the channel width $\tau_k$:

$$\tau_k = \frac{N_1 - N_2}{T_1 - T_2} = \frac{N}{T} \qquad (7.1.1)$$

In our case, for the necessary accuracy to be obtained the difference $(N_1 - N_2)$ should be $\sim$ 2000 channels. The relative accuracy of determining the channel width will be found as:

$$\delta \tau_k = \left[\delta^2_N + \delta^2_T\right]^{1/2} = 0.025\ \% \qquad (7.1.2)$$

The value of the absolute error in the determination of the difference of the peak positions in the analyser was $\pm$0.330 and $\pm$0.082 ns in the first and second steps, respectively. The relative error in the determination of the calibrated time interval $\delta_T$ was equal to $1 \times 10^{-8}$. (The integral and differential non-linearities of the spectrometer were thus taken into account).

## 7.2. Determination of the position of the "zero time"

Special attention was devoted to the determination of the "zero time" since the uranium chambers are not sensitive to fission gamma quanta. Three independent methods were used to determine the "zero time".

1. Signals from the nanosecond pulse generator (NPG) were sent simultanenously to the current collecting electrodes of the uranium and californium chambers (see Fig. 10). The shape of the signals was close to that of the pulses from the U-235 and

Cf-252 fission fragments. The position of the reference peak on the analyser time scale determined the position of the "zero time". Whether this position was true or not was checked by varying the amplitudes of the current signal sent to the chamber electrodes. The signal was varied in each chamber separately within the dynamic range of amplitude distribution of pulses from fission fragments (see Figs. 4 and 9). In this case, the position of the reference peak did not change and the accuracy of determination was $\pm 0.5$ channels ($\tau_{k1}$ = = 0.658 ns, $\tau_{k2}$ = 0.1645 ns are $\tau_k$ for the first and second measurements steps respectively).

2. We made a special chamber in which four electrodes with uranium layers were replaced by pure backings, while the fifth electrode was shaped like a disc with uranium layer 10 mm in diameter located at the centre of the pure backing. This electrode occupied the outermost position in the chamber. The electrical properties of this chamber were identical with those of the working uranium chambers. During measurements the californium chamber was located in the immediate vicinity of the special chamber. The average distance from the californium layer and the uranium layer was $\sim 6$ mm. In such a geometry and for the working thresholds of the discriminator we obtained the neutron time-of-flight spectrum. The distribution half-width was 1.61 ns. Introducing corrections for the time resolution of the spectrometer (1.32 ns) and for the time-of-flight of neutrons, we obtained the position of the "zero time", which agreed with that obtained by the first method with an accuracy of up to $\pm 0.08$ ns.

3. The third method involves comparison of experimental energy spectrum data obtained after making all corrections for the various flight path lengths. For this purpose, we derived the following values:

$$X_1^2 = \sum_i^n \frac{(N_{25i} - N_{50i})^2}{(N_{25i} + N_{50i})}; \quad X_2^2 = \sum_i^n \frac{(N_{50i} - N_{100i})^2}{(N_{50i} + N_{100i})};$$

$$X_3^2 = \sum_i^n \frac{(N_{25i} - N_{100i})^2}{(N_{25i} + N_{100i})},$$

where $N_{25i}$, $N_{50i}$, $N_{100i}$ are the experimental values of the spectrum intensity in the i-th channel for the corresponding path length. By varying the position of the "zero" time on the analyser time scale we found min $(X_1^2 + X_2^2 + X_3^2)$. Thus we confirmed the initial position of the "zero" time obtained by reference peak method with an accuracy of $\pm$0.45 ns and $\pm$0.102 ns for the first and second measurement steps, respectively.

## 7.3. Spectrometer time resolution

The time resolution of the spectrometer is determined by that of the californium and uranium chambers. In order to measure the latter, we used a gamma-quantum detector based on a plastic scintillator (Ø 15 mm) and a photomultiplier FEU-87. Measurement of the peak half-width for coincidence of two gamma-quanta from a Co-60 source at a threshold of $\sim$960 keV with the use of two such gamma detectors showed that their intrinsic resolution was 0.22$\pm$0.01 ns.

By measuring the half-width of the gamma peak obtained for the coincidence of pulses from Cf-252 fission fragments and prompt fission gamma quanta we obtained the time resolution of the californium chamber as 0.51$\pm$0.02 ns.

In order to determine the time resolution of the working uranium chamber, we prepared an identical chamber where one of the plates contained Cf-252 embedded uniformly in the U-235 layer. The amplitude characteristics of this chamber were close to those of the working chambers. The measurement results showed that instrinsic resolution of the working chamber was 1.22$\pm$ $\pm$0.02 ns.

The total time resolution of the spectrometer was 1.32$\pm$ $\pm$0.02 ns.

## 7.4. Efficiency of the spectrometer

The neutron registration efficiency is determined by the U-235 fission cross-section, the uncertainty in the value of which does not exceed ~4 % in the whole energy range. We used the data on the cross-section of the reaction from the ENDF/B-V file /2/. The great advantage of the uranium chamber over detectors of other types was that there was no possibility of detecting neutrons from any other reactions for uranium or other elements contained in the structural materials. The chamber was so designed that the corrections for the scattering of neutrons from the chamber walls were small and could be taken into account easily by calculation using the approximation of single interaction (the values of this correction will be given in Section 10).

The experimental determination of the average neutron registration efficiency for the spectra of Cf-252 fission neutrons was performed under working conditions at two intensities of the californium layers ($5 \times 10^5$ and $5 \times 10^4$ fissions/s) so that we had an accurate correction for the dead time in the "STOP" channels.

$$\varepsilon_{exp} = \frac{N_{on}}{N_o \bar{\nu}} = (6.48 \pm 0.06) \cdot 10^{-8}, \qquad (7.4.1)$$

where $N_o$ is the number of fissions in the californium layer, $\bar{\nu}$-the number of neutrons per fission event and $N_{on}$-the number of fragment - neutron coincidences in the entire energy region. The measurements are performed at a flight length of 50 cm.

Using the evaluated data on the average cross-section ($\bar{\sigma}cf$) we can calculate the neutron detection efficiency for the Cf-252 neutron spectrum

$$\varepsilon_{calc} = \frac{\bar{\sigma}_{cf} N_o}{4\pi L^2} = (8.11 \pm 0.13) \cdot 10^{-8}, \qquad (7.4.2)$$

where $N_o$ is the number of uranium atoms in the chamber, L-the flight length equal to 50 cm and $\bar{\sigma}cf$-the average cross-section

of U-235 fission induced by Cf-252 spontaneous fission neutrons ($\bar{\sigma}$cf = 1216±20 mb /21/).

Since not all fragments are registered in the chamber, it was necessary to take into account the corrections for absorption in the layer, anisotropy and kinematic effects and also necessity to record fragments at the non-zero threshold (in order to cut off alpha particles and noise). The absorption of fragments in the layer, an anisotropy and kinematic effects can be determined by the formula from Ref /22/:

$$\bar{K} = \frac{K_R + K_Y}{2} = \frac{3}{3 + a}\left(\frac{d}{l} + \alpha + \frac{2\alpha^2 l}{d}\right). \quad \alpha = \sqrt{\frac{E_n}{E_f}} \cdot \frac{\sqrt{A_f}}{A + 1} \tag{7.4.3}$$

where $K_R$ is the contribution to $\bar{K}$ in the case of uranium nuclei knocked into the target, $K_Y$ the contribution to K in the case of uranium nuclei knocked out of the tatget, a - an anisotropy, which depends on neutron energy, the data being taken from Refs /23, 24/; d-the uranium layer average thickness equal to 1.09± ±0.05 mg/cm$^2$; l-the path of the average fragment in the $U_3O_8$ layer equal to 5.9 mg/cm$^2$ /25/; $E_n$ - the incident neutron energy, MeV; $E_f$ - the average kinetic energy of the U-235 fission fragments equal to 80 MeV; $A_f$ - the average fragment mass equal to 118 and A the atomic number of U-235.

The spectrum-average value for the correction K is 12.64 %. The correction for the fragments of detecting threshold reduces the efficiency further by 7.3 %. The final fragment regictration efficiency in the chamber is ~ 80 %.

Thus, by introducing corrections for the fragment registration efficiency into the colculated efficiency of the spectrometer, we obtain good agreement with the experimental efficiency; this confirms that there are no effects unaccounted for in the operation of the equipment.

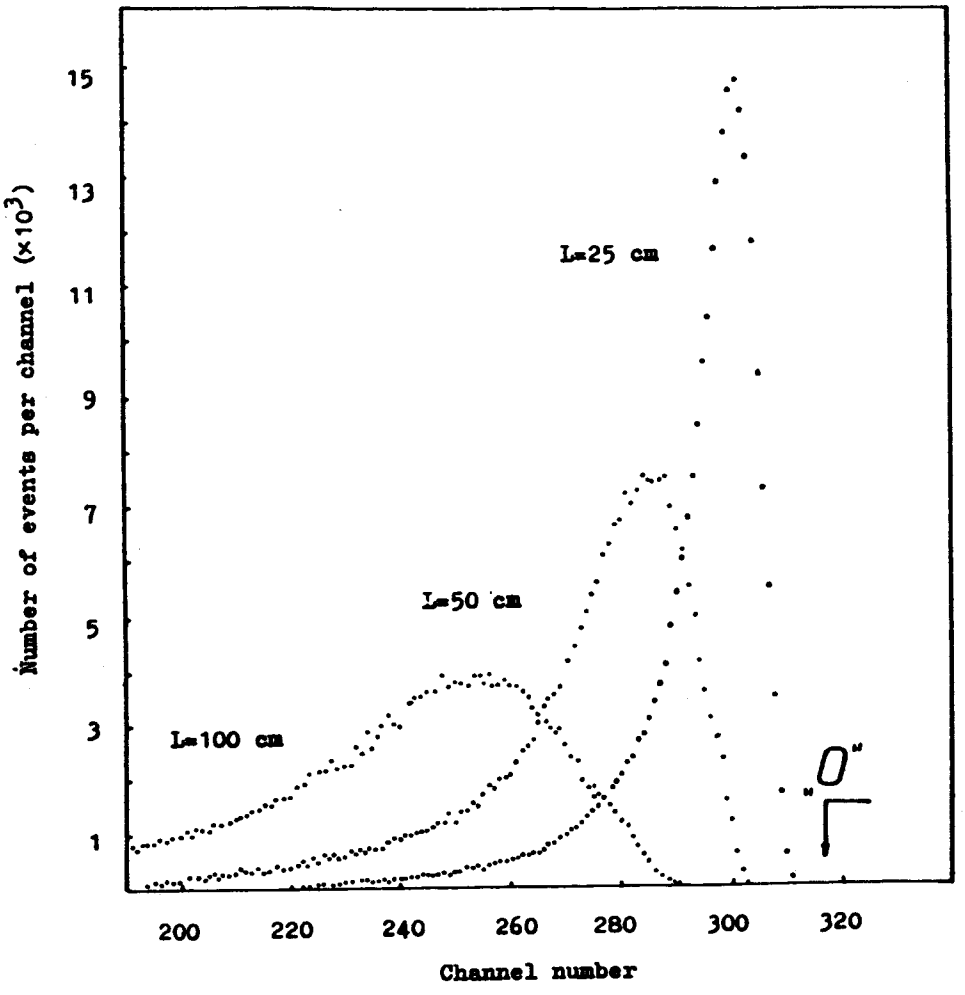


Figure 14 Time-of-flight spectra at three path lengths - 25, 50 and 100 cm.

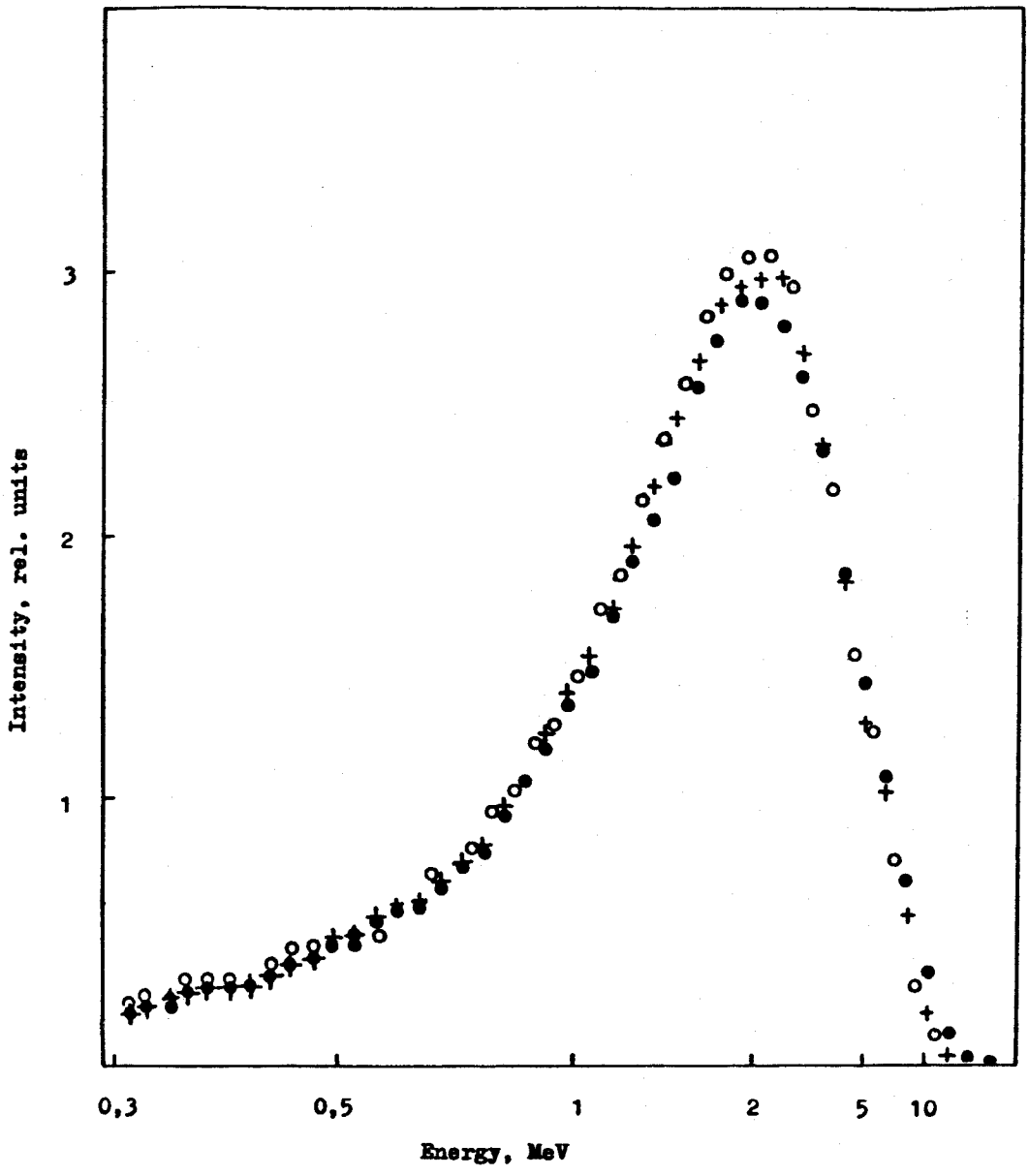


Figure 15 Time-of-flight spectra at three path lengths - 25, 50 and 100 cm - normalized to one integral:
●- 25 cm; + - 50 cm; o- 100 cm.

## 8. MEASUREMENTS

The Cf-252 spontaneous fission neutron spectrum was measured at the first stage with four chambers in an experimental hall 500 $m^3$ (see Figure 10). The spectrum obtained from each chamber was recorded into the corresponding analyser memory, where we also recorded the reference peak which was used to check the stability of the position of the "zero" time in each channel with an accuracy of up to ±0.3 ns. The measurements were carried out at three flight path lengths of 25, 50 and 100 cm for 2, 4 and 10 days, respectively. The spectrum was measured twice at each path length. Different path lehgths were used to check the proper operation of the facility and the corrections introduced (for backgrounds, scattered neutrons etc). The spectra are usually measured at one path length. In such measurements it is difficult to detect possible unaccounted-for errors associated with time shift.

At the second stage the measurements were performed outdoors, at a height of eight metres from the ground surface and away from objects producing scatter, under conditions which ruled out the effect of atmospheric precipitation at moderate humidity. The random coincidence background at this measurement stage was lower than during the first one by a factor of 4.6 . In order to obtain a higher accuracy of the time position of the spectrum, we performed the measurements with one chamber. The channel width was reduced to 0.1645 ns. Since we used one uranium chamber, the efficiency also diminished by a factor of 4. The measurements were done at two path lengths, 25 and 50 cm, for 2 and 21 days respectively. At the 50 cm path length the measurements were performed in three series of seven days each, in which time the reference peak shifted by not more than ±0.082 ns. Figures 14 and 15 give the instrument spectra obtained at path lengths of 25, 50 and 100 cm in the first measurement step. Figure 16 shows the instrument spectrum of neutrons at a path length of 50 cm in the second measurement step. The latter figure also gives the calculated background

without the pile-up rejector (curve c), the random background (curve a) and the calculated background with the pile-up rejector (curve b). It will be seen from this figure that the maximum remaining background due to the dead time ($\varepsilon_M$) is 3.0 % of the effect at 700 keV and becomes zero at energies below 300 keV. Without the pile-up rejector the background would be equal to the effect at ~ 100 keV.

## 9. PROCESSING OF THE EXPERIMENTAL DATA

The measurement results were processed for each flight length separately. The results of the individual series for each flight length were summed. As a first approximation the position of the reference peak (its location was described in Section 7.2) served as the "zero" time. In the case of each analyser channel for the measured spectrum we determined the time of flight and the corresponding energy of the neutron recorded in this channel. Since for energies above 1 MeV the correction for the relativistic effect becomes considerable the relation - ship between neutron energy and the time of flight of some path length L was determined from the expression

$$E_i = 939{,}57\left(\frac{1}{\sqrt{1 - \frac{L^2}{t_i^2 c^2}}} - 1\right), \qquad (9.1.1)$$

where $E_i$ is neutron energy MeV, $t_i$ is the time of flight ns, L the flight path length cm and c the velocity of light cm/ns.

The time spectrum was converted into the energy spectrum by the formula

$$N(E_i) = P\left[N_e(t_i) - \sum_j N_j(t_i)\right]\left(1 - \frac{L^2}{c^2 t_i^2}\right)^{3/2} t_i^3 / \left[L^2 \sigma_f(E_i)\right] \qquad (9.2)$$

where P is a normalized constant, $N_e(t_i)$ experimental intensity of the spectrum in i-th channel, $t_i$ the time in i-th channel ns,

L the flight path length cm, $\sigma(E_i)$ the U-235(n,f) cross section from the ENDF/B-V file and $N_i$ the following corrections:

1. Random coincidence background;
2. True-random coincidence background;
3. Kinematic effects and anisotropy;
4. Neutron scattering by air;
5. Scattering by the chambers;
6. Time resolution and uncertainty in path length.

## 10. CORRECTIONS

1. The correction for the random coincidence background was determined experimentally in each measurement separately with 800 channels before the "zero" time. The value of this correction depends on the neutron source strength, the intrinsic background of neutron detector and the scattered-neutron background.

2. The correction for the true-random coincidence background was determined by calculation from Eq. (6.3.2). The value of this background depends on the intensity of the californium layer, the deadtime of the fragment detector and the electronics, and also on the path length. For different path lengths this background is re-distributed into different energy intervals of the spectrum. Figure 16 shows the typical data on this background at a path length of 50 cm with (curve b) and without (curve c) the rejector.

3. The correction for anisotropy and kinematic effects was obtained by the formula (7.4.3) and the calculation results are shown in Table 1.

Table 1

| $E_{(MeV)}$ | 0,18 | 0,25 | 0,5 | 1,0 | 1,5 | 2,0 | 6,0 | 6,5 | 6,8 | 9,0 | 10 |
|---|---|---|---|---|---|---|---|---|---|---|---|
| $\bar{K}$ (%) | 14,0 | 13,8 | 13,5 | 13,0 | 12,7 | 12,3 | 12,3 | 12,0 | 11,1 | 10,8 | 10,7 |

4. The correction for neutron scattering by air was determined by calculation by the method described in Ref /26/. Neutrons of the initial spectrum $N_M$ are emitted from a source located at a distance of $\ell$ from the isotropic detector. As the initial spectrum we used the fission neutron time-of-flight distribution with the spectrum described by the Maxwell formula with the parameter T = 1.42 MeV. The time distribution detected can be represented as the superposition of two spectra: the spectrum of neutrons which passed through a layer of air with a thickness of $\ell$ $N_1(t)$ and are scattered by the surrounding medium into the detector $N_2(t)$:

$$N_1(t) = N_M(t)\left\{1 - \left[\rho_1\sigma_1(t) + \rho_2\sigma_2(t)\right]l\right\}\varepsilon(t)$$

$$N_2(t) = \frac{S}{8\pi}\sum_i^2 \int_o^{\pi} \int_o^{2_{max}} \int_{t_{min}}^{t_{max}} \frac{\rho_i \sin\alpha}{K_i r_i^2}\sigma_i(0,\tau)N_M\cdot\varepsilon(\tau)\delta(t - K_i\tau) \times$$

$$\times \, dr d\tau d\alpha$$

where $P_1$ and $P_2$ are the densities of the nitrogen and oxygen nuclei in air under normal conditions; $\sigma_1(\theta,\tau)$ and $\sigma_2(\theta,\tau)$ are the differential neutron scattering cross-sections for the nitrogen and oxygen nuclei /27/; S is the area of the isotropic detector; $\varepsilon(\tau)$ is the detector's neutron recording efficiency; r and $r_1$ are the flight lengths from the source to the point of scattering and from the point of scattering to the detector, respectively; $K_i = (a_i r_i + r)/\ell$ is the neutron energy independent coefficent of increase in neutron time-of-flight during scattering ($a_i$ takes into account the change in neutron velocity during scattering at an angle of $\theta$); $\alpha$ is the angle of neutron emission from the source. The recorded $(N_1 + N_2)$ spectrum and its deviation from the initial spectrum $\frac{N_1 + N_2}{N_M}\cdot 100\ \%$ is shown in Figure 17. The calculation was carried out on a computer for three path lengths - 25, 50 and 100 cm. The result is shown in Figure 17.

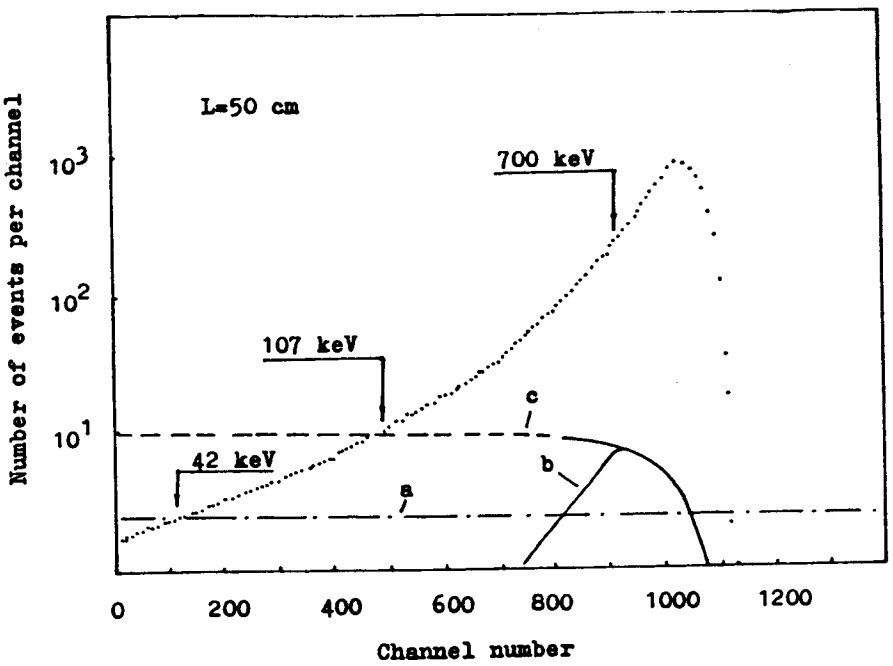


Figure 16 The typical instrument spectrum in the second measurement step at a path length of 50 cm (curve d), calculated background without the pile-up rejector (curve c), the remaining background with the pile-up rejector (curve b), random coincidence background (curve a).

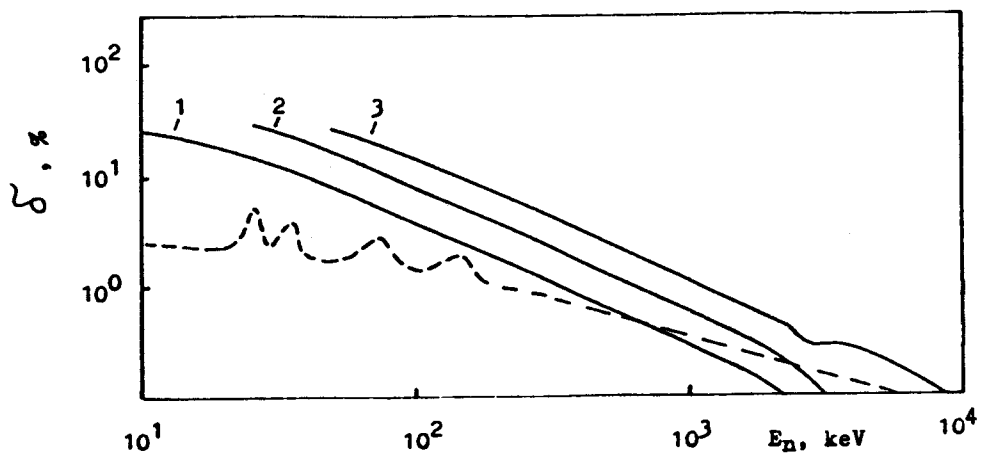


Figure 17 Correction functions for neutron scattering by air (continuous curves) and by detectors (dashed curve) for flight lengths: (1) - 25 cm; (2) - 50 cm; (3) - 100 cm.

5. The corrections for the scattering by the chambers was obtained by calculations. For that purpose, the method described in Ref /14/ was used. Since the current ionization chambers for both neutron source and detector were intentionally so designed as to have smaller masses, the corrections for neutron scattering by the chambers were small in value. It was therefore quite sufficient to perform a simple calculation in order to obtain them. The calculation results are shown in Fig. 17, from where it will be seen that the value of the maximum correction is less than 3 %, and the approximation used did not therefore introduce substantial errors.

6. The correction for time resolution and for uncertainty in the path length (H) was determined by calculation. The initial spectrum was taken as a first approximation in the form of a Maxwellian distribution ($N(E) \sim c\sqrt{E}\, e^{-E}/T$ with T = = 1.42 MeV.)This spectrum was then distorted by introducing the resolution function:

$$\varphi(t) = \frac{1}{\sqrt{2\pi}2\sigma_{\Delta L}} e^{-\frac{(t - t_o)^2}{\sigma^2}}, \quad \sigma = \frac{\Delta t}{2{,}355} \qquad (10.1)$$

where $\Delta t = 1.32 \pm 0.02$ ns is the time resolution of the spectrometer. The distorted spectrum was determined as

$$N(t_o) = \frac{2{,}355}{2\Delta L \Delta t \sqrt{2\pi}} \int_{L-\Delta L}^{L+\Delta L} dL \int_{t_o-\Delta t}^{t_o+3\Delta t} \sigma_f(E)\sqrt{\frac{E}{T}} e^{-E/T} e^{-\frac{2{,}773(t-t_o)^2}{\Delta t^2}} \frac{dt}{t} \qquad (10.2)$$

where $\sigma_f(E)$ is the U-235 fission cross-section and $\Delta L$ the uncertainty of the flight length. The integration was carried out numerically by the Simpson formula. Since the shape of the measured neutron spectrum, starting from an energy higher than 5 MeV, deviated systematically from the Maxwellian distribution, as a second approximation the correction H was determined with the help of the initial spectrum in the form

$$N(E) \sim \left[1 - 0.047(E - 4.8)\right] \sqrt{E}\, \exp(-\frac{E}{T}), \qquad (10.3)$$

where T = 1.42 MeV. ($E \gtrsim 4.8$ MeV).

The value of this correction at a flight length of 50.00$\pm$ $\pm$0.25 cm and for a time resolution of t = 1.32 ns as a function of neutron energy is illustrated in Table 2.

Table 2

| E MeV | 10.31 | 9.46 | 8.71 | 8.04 | 7.45 | 6.92 | 6.28 | 5.86 |
|---|---|---|---|---|---|---|---|---|
| H | 1.151 | 1.092 | 1.039 | 0.988 | 0.957 | 0.961 | 0.998 | 1.050 |

| E MeV | 5.49 | 5.15 | 4.84 | 4.64 | 4.42 | 3.74 | 2.78 | 1.16 | 0.506 |
|---|---|---|---|---|---|---|---|---|---|
| H | 1.027 | 1.010 | 0.999 | 0.994 | 0.998 | 0.995 | 0.995 | 1.001 | 1.001 |

## 11. ERRORS

The relative error in the value of the intensity of the measured spectrum for a given energy was determined from formula 9.2 in the form (without considering the relativistic correction):

$$\delta N(E_i) \simeq \left\{ {}^2N_{st.i} + \sum_i \delta^2 K_{ji} + 4\delta^2 L(1 + \frac{\partial \sigma_i}{\partial E_i}\frac{E_i}{\sigma_i})^2 + \delta^2 \sigma_f + \right.$$

$$\left. + \delta^2 t_i \left[(3 + 2\frac{\partial \sigma_i}{\partial E_i}\frac{E_i}{\sigma_i})^2 + t_i^2(\frac{\partial N_{ei}}{\partial t_i})^2 + \sum_i t_i^2(\frac{\partial K_{ji}}{\partial t_i})^2\right]\right\}^{1/2} \qquad (11.1)$$

where $\delta N_{st.i}$ is the statistical error in the i-th channel, $\delta K_{ij}$ - the error of the j-th correction, $\delta \sigma_i$ - the error in the U-235(n,f) reaction cross-section value from the ENDF/B-V file, $\delta t_i$ - the error of determination of the time of the i-th channel and $\delta L$ - the error in the path length, $N_{ei}$ - experimental intensity of the spectrum in i-th channel.

1. The statistical error in the i-th channel of the analyser was determined as

$$N_{st.i} = (N_{ei} + \bar{N}_b)^{1/2}/(N_{ei} - \bar{N}_b), \qquad (11.2)$$

where $N_{ei}$ is the number of counts in the i-th channel and $\bar{N}_b$ - the average value of the background.

2. The error in the determination of the correction for the true-random coincidence background was found from Eq. (6.2.2)

$$\delta M_i = (\delta^2 N_o + \delta^2 \tau_K + \sum_I \delta^2 N_{st.i})^{1/2} \qquad (11.3)$$

where $\delta N_o$ is the error in the determination of the number of recorded fragments on the californium chamber, $\delta \tau_K$ - the error in the determination of the value of the spectrometer channel and $\delta N_{st.i}$ - the statistical error.

3. The error in the determination of the correction for anisotropy and kinematic effects was found from the Eq. (7.4.3)

$$\delta \bar{K} = \left[\delta^2 a + \frac{(\frac{1}{l} - \frac{2\alpha^2 l}{d^2})^2}{(\frac{d}{l} - \alpha + \frac{2\alpha^2 l}{d})^2}\delta^2 d + \frac{(\frac{2\alpha^2}{d} - \frac{d}{l^2})^2}{(\frac{d}{p} - \alpha + \frac{2\alpha^2 l}{d})^2}\delta^2 l\right]^{1/2} \approx \delta a, \qquad (11.4)$$

The second and third terms are smaller than the first by more than two orders. d and l do not depend on energy; their errors will be: $\delta d = 4.6$ % and $\delta l = \pm 8{,}5$ % (for the notations see section 7.4, Eq. (7.4.3). At an anisotropy of "a" = 0.45 for $E_n = 10$ MeV the value of the error $\delta \bar{K}$ will equal 15.5 %. The energy dependence of $\delta \bar{K}$ will follow $\delta a$.

4. The error in the determination of the correction for neutron scattering by the structural material of the detectors $N_d$ and by the surrounding air $\delta N_a$ was associated with the uncertainty of the nuclear data used in the calculation and

with the approximate nature of the calculations. It was equal to ~ 25 % in the whole energy region /14/.

5. The error in the determination of the correction for time resolution and for uncertainty in the path length was obtained by calculation using the variations $\delta t$ and $\delta L$ in expression (10.2) ($\delta tL$). The error in the determination of the time resolution and path length was taken as ~ 10 % and ~0.5 % respectively (for a flight length of 50 cm). It is shown in Table 3.

Table 3

| E, MeV | 10.5 | 9.7 | 8.9 | 8.2 | 7.6 | 7.0 | 6.6 | 6.1 |
|---|---|---|---|---|---|---|---|---|
| $\delta$ H % | 2.6 | 1.8 | 0.5 | 0.3 | 0.8 | 0.7 | 0.5 | 0.3 |

| E, MeV | 5.9 | 5.5 | 5.1 | 4.4 | 4.0 | 2.8 | 2.0 | 0.6 |
|---|---|---|---|---|---|---|---|---|
| $\delta$ H % | 0.8 | 0.5 | 0.3 | 0.3 | 0.2 | 0.2 | 0.1 | 0.05 |

6. The error in the value of efficiency $\varepsilon(E)$ is determined by the error in the value of the U-235(n,f) reaction cross-section which was taken from the ENDF/B-V file.

7. The error in the determination of the time-of-flight ($\delta t_i$) is determined as

$$\delta t_i = (\delta^2 \tau_K + \delta^2 t_{oi})^{1/2}, \qquad (11.5)$$

where $\delta \tau_K$ = 0.07 % is the error in the value of the channel, $\delta t_{oi} = \frac{\Delta t_o}{ti}$ is the relative error in the position of the "zero" time, $\Delta t_o = \pm 0.08$ ns the absolute error in the "zero" time.

In order to illustrate the contribution of the error in the determination of the zero time to the value of $\delta$ N, we carried out a calculation for a flight path length of 50 cm, in which specified $\Delta t_o = \pm 0.08$ ns. The value of $\delta$ N as a function of energy is shown in Table 4.

Table 4

| $\delta$N, % | 4.8 | 3.7 | 3.0 | 2.3 | 1.9 | 1.6 | 1.5 | 1.25 |
|---|---|---|---|---|---|---|---|---|
| E, MeV | 9.9 | 8.4 | 7.2 | 6.3 | 5.5 | 4.9 | 4.5 | 4.2 |

| $\delta$N, % | 1.1 | 1.0 | 0.8 | 0.7 | 0.6 | 0.5 | 0.4 | 0.1 |
|---|---|---|---|---|---|---|---|---|
| E, MeV | 3.9 | 3.1 | 2.8 | 2.2 | 1.8 | 1.5 | 1.0 | 0.5 |

8. The error in the determination of path length $\delta_L = \frac{\Delta' L}{L}$ was due to the inaccuracy of determining the path length and to the transport of californium from the backing to the current-collecting electrode under the influence of the applied voltage and amounted to not more than 0.5 %

9. The relative error in the determination of neutron energy was calculated by the formula

$$\delta E_i = 2(\delta_0^2 L + \delta_0^2 ti)^{1/2} \qquad (11.6)$$

where $\delta_0 L = \frac{\Delta L}{L}$, $\Delta L = \left[(\Delta' L)^2 + (\Delta'' L)^2\right]^{1/2}$.
$\Delta' L$ was determined earlier; $\Delta'' L$, the uncertainty in path length, which is determined by the uranium chamber thickness (equal to 12 mm); $\delta_0 ti = (\delta^2 ti + \delta^2 ti^1)^{1/2}$: $\delta ti$ - was determined earlier (see formula 11.1), $\delta ti^1$ - is the uncertainty of time $t_1$ associated with the time resolution of the spectrometer (see Section 7.3).

## 12. RESULTS

After introducing all the corrections into the experimental data obtained for different flight path lengths, we compared the spectra with each other (the data were normalized to one of the integrals). A typical result for comparison of data obtained at flight lengths of 25 and 50 cm in the second measurement step is shown in Figure 18. It will be seen from the

figure that the agreement is fully satisfactory in the whole measurement range.

The final result was obtained by averaging the values of spectrum intensities from measurements in the different steps and at the various path lengths with allowance for the weights of partial errors. In the low-energy region the data were taken mainly from the first measurement step at a flight length of 25 cm, and in the case of the medium and high-energy region, from the second measurement step at a flight length of 50 cm.

Table 5 presents the numerical data on the spectrum for 79 energy groups (0.01-11 MeV) in the form of the ratio $\mu(E) = \frac{Ne(E)}{Nc(E)}$ where Ne(E) denotes experimental data and Nc(E) = $= c\sqrt{E}\exp(-E/T)$ (T = 1.42 MeV) is the calculated Maxwellian spectrum. Table 5 gives also the total error for each energy group. The obtained experimental errors (3-5 %) are commensurate with the errors in the U-235(n,f) reaction cross-section (2.5-4 %), and therefore any further increase in measurement accuracy would not have refined the final result significantly. The value of the average spectrum energy was found to be 2.116 MeV in the 0.01-10 MeV region.

The experimental results obtained in the second measurements step can be recommended for use in evaluation of the Cf-252 spontaneous fission neutron spectrum, since these have a higher energy resolution and lower background than the data of the first step. The experimental results are given in Table 6 in the form of the ratio $\mu(E)$. The experimental and calculated data are normalized to one of the integrals in the 0.04-10 MeV region. Table 6 also contains the statistical errors. Table 7 gives the complete error file for second measurement step for eight energy groups, within which the values of the errors represent linear interpolation with the neighbouring groups. In the graph of the U-235 cross-section error the data for the 0.10-10 MeV region are taken from ENDF/B-V and those for the region below 0.10 MeV from Ref /28/. The cross-section of the U-235(n,f) reaction below 0.10 MeV is not a standard cross-section and does not have an error correlation matrix.

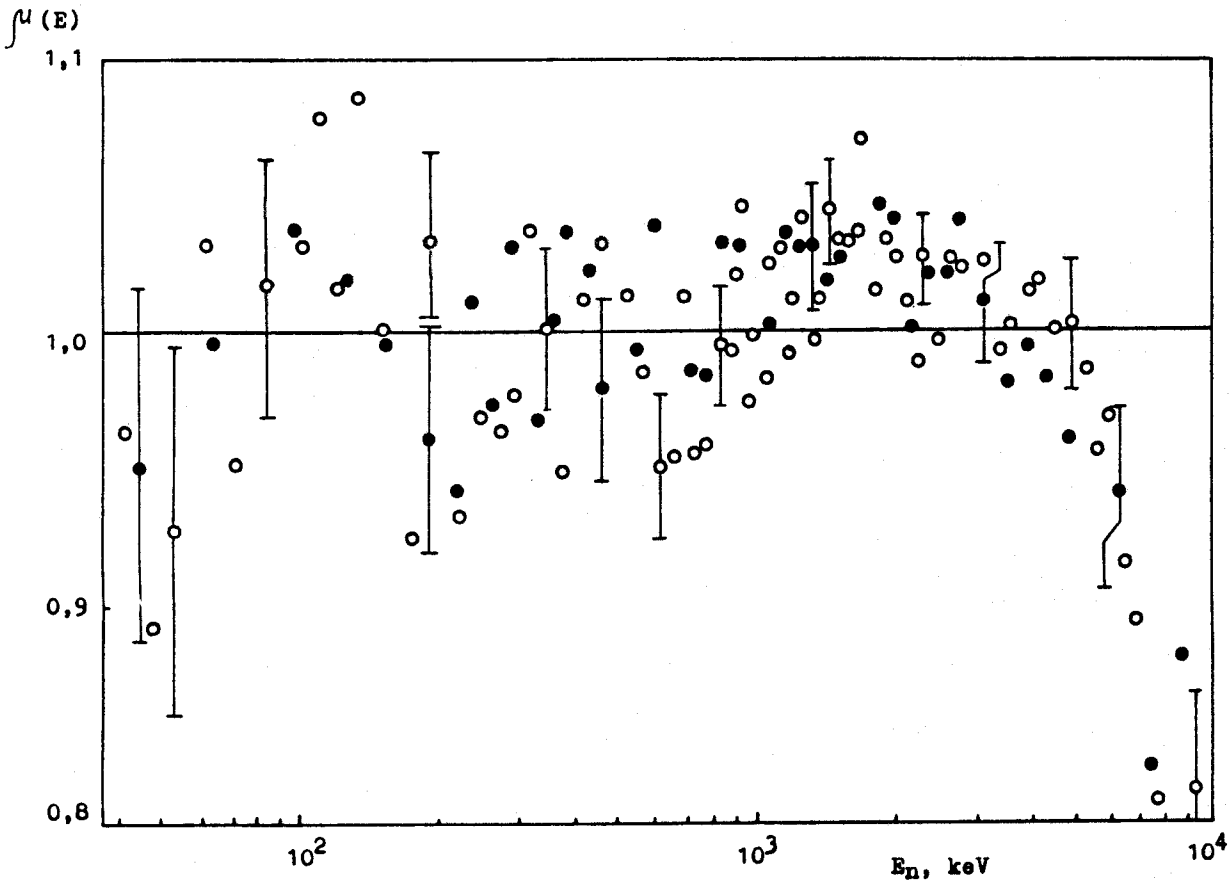


Figure 18 The ratio of experimental data to the Maxwellian distribution with T = 1.42 MeV (in the second measurement step: ● - path length 25 cm; ○ - path length 50 cm).

Table 5

Experimental data from two measurements steps in the form of the ratio $\mu(E) = \frac{Ne(E)}{Nc(E)}$

| E, MeV | $\mu(E)$ | $\delta$Ne, % | E, MeV | $\mu(E)$ | $\delta$Ne, % |
|---|---|---|---|---|---|
| 11.360 | 0.880 | 8.5 | 0.966 | 0.981 | 4.1 |
| 9.054 | 0.851 | 6.3 | 0.932 | 1.037 | 4.1 |
| 7.721 | 0.832 | 5.8 | 0.900 | 1.025 | 4.2 |
| 6.886 | 0.893 | 5.3 | 0.870 | 1.000 | 4.2 |
| 6.415 | 0.920 | 5.1 | 0.828 | 0.994 | 4.1 |
| 5.991 | 0.959 | 5.0 | 0.776 | 0.964 | 4.1 |
| 5.608 | 0.954 | 4.8 | 0.728 | 0.969 | 4.1 |
| 5.261 | 0.980 | 4.8 | 0.685 | 1.005 | 4.2 |
| 4.898 | 0.995 | 4.5 | 0.645 | 0.965 | 4.2 |
| 4.524 | 1.002 | 4.3 | 0.609 | 0.980 | 4.2 |
| 4.192 | 1.015 | 4.2 | 0.561 | 0.990 | 4.0 |
| 3.895 | 1.011 | 3.7 | 0.505 | 1.013 | 4.0 |
| 3.629 | 1.007 | 3.6 | 0.456 | 1.025 | 4.0 |
| 3.389 | 0.990 | 3.5 | 0.414 | 1.015 | 4.1 |
| 3.172 | 1.020 | 3.5 | 0.378 | 0.975 | 4.2 |
| 2.975 | 1.028 | 3.4 | 0.346 | 1.005 | 4.2 |
| 2.797 | 1.023 | 3.4 | 0.318 | 1.010 | 4.3 |
| 2.634 | 1.023 | 3.4 | 0.293 | 0.991 | 4.3 |
| 2.484 | 1.005 | 3.4 | 0.272 | 0.967 | 4.4 |
| 2.347 | 1.025 | 3.4 | 0.248 | 0.981 | 4.5 |
| 2.221 | 0.993 | 3.5 | 0.220 | 0.936 | 4.5 |
| 2.105 | 1.011 | 3.5 | 0.192 | 1.000 | 4.5 |
| 1.998 | 1.025 | 3.2 | 0.170 | 0.960 | 4.5 |
| 1.899 | 1.035 | 3.0 | 0.151 | 0.999 | 4.5 |
| 1.807 | 1.017 | 3.0 | 0.136 | 1.040 | 4.7 |
| 1.722 | 1.052 | 3.0 | 0.122 | 1.017 | 4.8 |
| 1.642 | 1.036 | 3.0 | 0.110 | 1.038 | 4.8 |
| 1.568 | 1.034 | 3.0 | 0.098 | 1.021 | 4.9 |
| 1.499 | 1.030 | 3.0 | 0.084 | 1.015 | 6.6 |
| 1.434 | 1.039 | 3.0 | 0.071 | 0.971 | 6.7 |
| 1.373 | 1.015 | 3.1 | 0.061 | 0.999 | 6.7 |
| 1.316 | 1.005 | 3.1 | 0.053 | 0.940 | 6.7 |
| 1.263 | 1.037 | 3.1 | 0.047 | 0.931 | 6.7 |
| 1.213 | 1.015 | 3.1 | 0.041 | 0.952 | 6.8 |
| 1.166 | 1.010 | 3.1 | 0.034 | 0.921 | 6.8 |
| 1.121 | 1.030 | 3.1 | 0.029 | 1.020 | 7.1 |
| 1.079 | 1.021 | 3.2 | 0.025 | 0.964 | 7.4 |
| 1.039 | 0.990 | 3.2 | 0.020 | 1.000 | 7.8 |
| 1.002 | 1.000 | 3.3 | 0.016 | 0.926 | 8.5 |
| | | | 0.012 | 0.963 | 11.6 |

Table 6

Experimental data from the second measurement step (path length 50 cm) in the form of the ratio

$$\mu(E) = \frac{Ne(E)}{Nc(E)}$$

| E, MeV | $\mu(E)$ | $\delta N_{st}$, % | E, MeV | $\mu(E)$ | $\delta N_{st}$, % |
|---|---|---|---|---|---|
| 11.360 | 0.847 | 4.6 | 0.966 | 0.974 | 2.7 |
| 9.054 | 0.831 | 3.5 | 0.932 | 1.045 | 2.7 |
| 7.721 | 0.827 | 3.4 | 0.900 | 1.020 | 2.8 |
| 6.886 | 0.893 | 3.3 | 0.870 | 0.992 | 2.9 |
| 6.415 | 0.913 | 3.2 | 0.828 | 0.994 | 2.2 |
| 5.991 | 0.968 | 3.0 | 0.776 | 0.958 | 2.3 |
| 5.608 | 0.954 | 3.0 | 0.728 | 0.957 | 2.4 |
| 5.261 | 0.984 | 2.8 | 0.685 | 1.013 | 2.4 |
| 4.898 | 1.002 | 2.3 | 0.645 | 0.954 | 2.6 |
| 4.524 | 1.000 | 2.1 | 0.609 | 0.949 | 2.7 |
| 4.192 | 1.019 | 2.0 | 0.561 | 0.985 | 2.0 |
| 3.895 | 1.015 | 1.9 | 0.505 | 1.013 | 2.2 |
| 3.629 | 1.007 | 1.9 | 0.456 | 1.032 | 2.3 |
| 3.389 | 0.993 | 1.8 | 0.414 | 1.011 | 2.5 |
| 3.172 | 1.024 | 1.8 | 0.378 | 0.949 | 2.8 |
| 2.975 | 1.025 | 1.7 | 0.346 | 1.008 | 2.9 |
| 2.797 | 1.023 | 1.7 | 0.318 | 1.037 | 3.1 |
| 2.634 | 1.026 | 1.7 | 0.293 | 0.976 | 3.4 |
| 2.484 | 0.997 | 1.7 | 0.272 | 0.963 | 3.6 |
| 2.347 | 1.027 | 1.7 | 0.248 | 0.968 | 3.2 |
| 2.221 | 0.988 | 1.8 | 0.220 | 0.932 | 3.1 |
| 2.105 | 1.010 | 1.8 | 0.192 | 1.033 | 3.3 |
| 1.998 | 1.027 | 1.8 | 0.170 | 0.925 | 3.8 |
| 1.899 | 1.033 | 1.8 | 0.151 | 1.002 | 4.0 |
| 1.807 | 1.017 | 1.8 | 0.136 | 1.086 | 4.2 |
| 1.722 | 1.070 | 1.8 | 0.122 | 1.017 | 4.8 |
| 1.642 | 1.036 | 1.9 | 0.110 | 1.079 | 5.1 |
| 1.568 | 1.034 | 2.0 | 0.098 | 1.031 | 4.7 |
| 1.499 | 1.033 | 2.0 | 0.084 | 1.017 | 4.7 |
| 1.434 | 1.043 | 2.0 | 0.071 | 0.951 | 5.4 |
| 1.373 | 1.011 | 2.1 | 0.062 | 1.033 | 5.6 |
| 1.316 | 0.997 | 2.2 | 0.054 | 0.926 | 6.9 |
| 1.263 | 1.040 | 2.2 | 0.047 | 0.891 | 8.0 |
| 1.213 | 1.011 | 2.3 | 0.042 | 0.963 | 8.4 |
| 1.166 | 0.992 | 2.4 | | | |
| 1.121 | 1.029 | 2.4 | | | |
| 1.079 | 1.025 | 2.4 | | | |
| 1.039 | 0.982 | 2.5 | | | |
| 1.002 | 0.999 | 2.6 | | | |

Table 7

Experimental data error file

| Error Energy Group | $\Delta t_o$ | $\delta\tau_K$ | $\delta_L$ | $\delta\sigma_f$ | $\delta_H$ | $\delta_{Na}$ | $\delta_{\bar{N}b}$ | $\delta_M$ | $\delta_{N_{st.}}$ | $\delta_{Nd}$ | $\delta_{\bar{K}}$ |
|---|---|---|---|---|---|---|---|---|---|---|---|
| MeV | ns | % | % | % | % | % | % | % | % | % | % |
| 8-10 | ±0.08 | 0.07 | 0.5 | 3.5 | 1.2 | 0 | 0 | 0 | 4 | 0 | 0.5 |
| 4-8 | ±0.08 | 0.07 | 0.5 | 3.5 | 1 | 0 | 0 | 0 | 2.2 | 0 | 0.3 |
| 2-4 | ±0.08 | 0.07 | 0.5 | 3.0 | 0.3 | 0 | 0, | 0 | 1.8 | 0 | 0.2 |
| 1-2 | ±0.08 | 0.07 | 0.5 | 2.5 | 0.1 | 0 | 0 | 0.05 | 1.8 | 0 | 0.15 |
| 0.4-1 | ±0.08 | 0.07 | 0.5 | 3.5 | 0 | 0.05 | 0 | 0.1 | 2.5 | 0 | 0 |
| 0.2-0.4 | ±0.08 | 0.07 | 0.5 | 3.0 | 0 | 0.2 | 0 | 0.05 | 3.5 | 0.5 | 0 |
| 0.1-0.2 | ±0.08 | 0.07 | 0.5 | 3.5 | 0 | 0.6 | 0.4 | 0 | 4.5 | 1 | 0 |
| 0.04-0.1 | ±0.08 | 0.07 | 0.5 | 6.0 | 0 | 1.5 | 2.5 | 0 | 6.5 | 1 | 0 |
| Correlation factor | 100 % | 100 % | 100 % | C*) | 100 % | 100 % | 100 % | 100 % | Not Correlated | 100 % | 100 % |

*) The values of the correlation factor C can be taken, for example, from Ref /24/, p.39

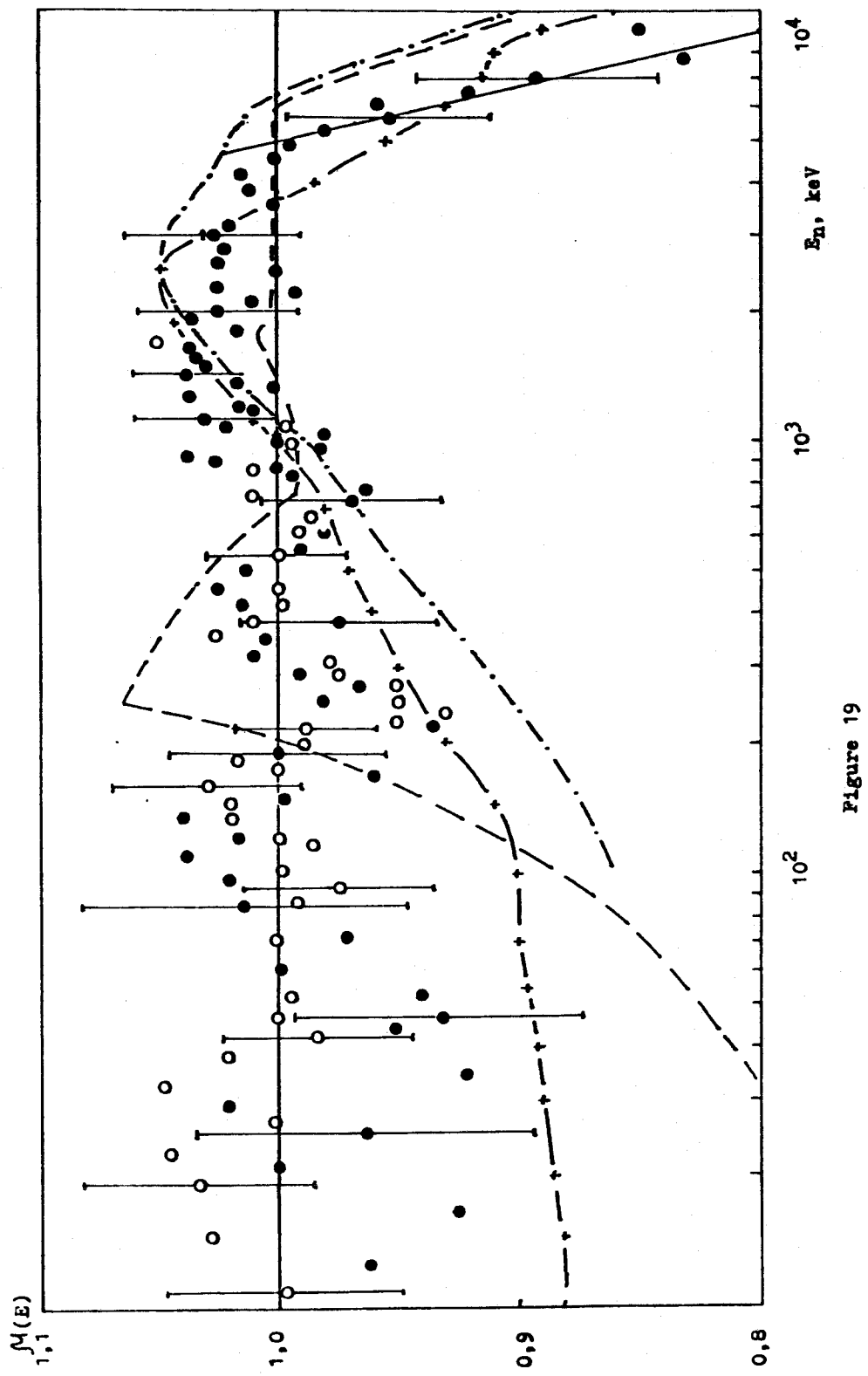


Figure 19 The experimental results obtained in the present study in the form of their ratio to the Maxwellian distribution (T = 1.42 MeV). The denoted errors are total errors. The dash curve represents the evaluation of Ref /1/, o-points are the data of Ref / 8/, the dot-dash curve is the data of Ref /9/, the continuous curve the data of Ref /10/ and +-the data of Ref /11/.

## 13. DISCUSSION OF RESULTS

For comparison of the obtained results with other data on the Cf-252 spontaneous fission neutron spectrum we give in Figure 19 the experimental data in the form of their ratio to the Maxwellian distribution:

$$N(E) \sim E^{1/2} e^{-E/T} \qquad (T = 1.42 \text{ MeV}) \qquad (13.1)$$

It will be seen from the figure that the measured spectrum agrees with an accuracy of ±5% with distribution (13.1) in the 10 keV - 5 MeV region. But the measured spectrum is slightly above the Maxwellian in the energy range 1 - 3 MeV (~ 2-3 %). In the case of higher energies, there is a systematic negative deviation from calculation, which goes up to ~15 % at 8 MeV.

There was some interest in comparing the obtained data with the results of Ref /8/, which had also been obtained at the V.G.Khlopin Radium Institute. In that study the measurements were made using another standard reaction Li-6(n,$\alpha$) in the 1 keV - 1 MeV region. It will be seen from Fig. 19 that the data as a whole agree satisfactorily. Some of the differences which exist are possibly associated with errors in the Li-6(n,$\alpha$) and U-235(n,f) cross-sections.

The results of the evaluation of Grundl and Eisenhauer /1/, in comparison with the data of the present study, are considerably lower (~20 %) in the low-energy region and sumewhat higher in the high-energy region (~5 % at $E_n$ = 10 MeV). The low-energy region in the evaluation was obtained by extrapolation of the spectrum from medium energies and cannot therefore claim a high accuracy. The high-energy region has recently been refined in Ref /4/, where the data were obtained with the highest energy resolution. The data of the latter study agree satisfactorily with those of ours in the high-energy region.

Figure 19 also gives the calculation results of Madland and Nix /9/, Märten et al. /10/ and Gerasimenko and Rubchenya /11/. The calculations in Ref /9,10/ were performed by the

evaporation model. Those in Refs /11/ were carried out by the Hauser-Feschbach theory. It may be noted that the results of these calculations /9, 10, 11/ agree satisfactorily with our data except for the low-energy region. The difference in this region is possibly due to the fact that the calculations omit the contribution of the yield of pre-equilibrim neutrons.

The authors express their sincere gratitude to V. I. Yurevich for calculating the corrections for neutron scattering by air, to B. M. Aleksandrov for preparing the californium layers, to P. S. Soloshenkov for preparing the U-235 layers and for helping in the study of the angular dependences of fragment yield from Cf-252 layers, to G. P. Tyurin for participating in developing the electronic blocks, to A. S. Veschikov for taking part in the construction of the fragment and neutron detectors and to N. A. Senyushkina for help with the measurements.

## REFERENCES


1. GRUNDL J. A., EISENHAUER C. M. Proc. Intern. Conf. on Nuclear Cross Sections and Technology, Washington, 1975, NBS Spec. publ. 425 (1975), vol. 1, p. 250.and IAEA-TECDOC-208 (1978), vol. 1, p. 53.
2. CULLEN D. E., KOCHEROV N. P., McLAAGHLIN, Nucl. Sci. Ing. 83 (1983) 497.
3. POENITZ W. P., TAMURA T. Proc. Intern. Conf. on Nuclear Data for Science and Technology Antwerp, 1982, Brussels, ECSC, EEC, EAEC, (1983), p. 465.
4. BÖTTGER R., KLEIN H., CHALUPKA A., STROHMEIER B. Ibid, p. 484.
5. MÄRTEN H., SEELIGER D., STOBINSKI B. Ibid, p. 488; INDC(GDR)-17/L, 1982.
6. BLINOV M. V., BOYKOV G. S., VITENKO V. A. Ibid, p. 479.
7. BATENKOV O. I., BLINOV M. V., BOYKOV G. S., VITENKO V. A., RUBCHENYA V. A. IAEA Consult. Meeting on $^{235}U$ Fast Neutron Fission Cross-Section and $^{252}Cf$ Fission Neutron Spectrum Smolenice, 1983, INDC(NDC)-146/L 1983, p. 161.
8. BLINOV M. V., VITENKO V. A., YUREVICH V. I. in: Nejtronnaya Fizika (Neutron Physics), part 3, Moscow (1980) 109; Zfk-40 (1980) 104.
9. MADLAND D. G., NIX J. R. Nucl. Sci. Eng. 81 (1982) 213 and in Ref. /3/ p. 473.
10. MÄRTEN H., NEUMANN D., SEELIGER D. In ref. /7/ p. 199.
11. GERASIMENKO B. F., RUBCHENYA V. A., Report RI-183 (1984) (in Russian).
12. INDC/NEANDC Nuclear Standards File Version 80 INDC-36/LN.
13. ALEKSANDROV B. M., KOROLEV E. V. et al., in: Nejtronnaya Fizika (Neutron Physics), part 4, Moscow (1980) 119.
14. CHULUPKA A. Nucl. Instr. Meth. 164 (1979) 105.
15. MAIER M. R., SPERR P. Nucl. Instr. Meth. 87 (1970) 13.
16. KORNILOV N. V. in: Nejtronnaya Fizika (Neutron Physics), part 6, Moscow (1976) 276.

17. CHERNYAVSKIJ A. F., BEKETOV S. V. et al., in: Statisticheskie metody analiza sluchajnykh signalov v jadernofizicheskom ehkśperimente (The Methods of Statistical Analysis of Random Signals in Nuclear Physics Experiments), Moscow (1974).
18. BLINOV M. V., VITENKO V. A., YUREVICH V. I., in: Nejtronnaya Fizika (Neutron Physics), part 4, Moscow (1980) 96.
19. BOJKOV G. S., VITENKO V. A., TYURIN G. P., in: Prikladnaya yadernaya spektroskopiya (Applied Nuclear Spectroscopy) N 13 Leningrad (1984) 189.
20. GREEN L., MITCHELL J. A., STEEN N. M. Nucl. Sci. Eng. 50 (1973) 257.
21. GRUNDE J., GILLIAM D., McGARRY D., EISENHAVER C., SORAN P. In ref. /7/ p. 237.
22. ARET R., PAUSCH G., TEICHNER R., WAGNER W. Preprint TU 05-5-79 Dresden (1979).
23. SMIRENNIN G. N., SHPAK D. L., OSTAPENKO Yu. B., FURSOV B. I. Pisma v JETP (Phys. JETP Lett) 11 (1970) 333.
24. KAPOOR S. S. Nuclear Data Standards for Nuclear Measurements (1982 INDC/NEANDC Nuclear Standards File) Vienna IAEA (1983) 47.
25. POENITZ W. P., MEADOWS J. W. In ref. /7/ p. 27.
26. IVANOV O. I., SAFONOV V. A., At.Energ. 36, 5 (1974) 397.
27. NIKOLAEV M. N., BAZAZYANTS N. O. Anizotropiya uprugorasseyannykh nejtronov (The Anisotropy of Elastically Scattered Neutrons), Atomizdat, Moscow (1972).
28. KON'SHIN V. A., ZHARKOV V. G., SUKHOVITSTIY E. Sh. INDC (CCCP)-148/L Vienna IAEA (1980).

1426.